UNIVERSITY OF THESSALY
SCHOOL OF ENGINEERING
DEPARTMENT OF MECHANICAL ENGINEERING

FINITE ELEMENT ANALYSIS OF LATERAL BUCKLING HP/HT OF OFFSHORE STEEL PIPELINES

by
AIKATERINI AFENTOULI

Submitted in partial fulfillment of the requirements for the degree of Diploma in Mechanical Engineering at the University of Thessaly

Volos, 2021

UNIVERSITY OF THESSALY
SCHOOL OF ENGINEERING
DEPARTMENT OF MECHANICAL ENGINEERING

FINITE ELEMENT ANALYSIS OF LATERAL BUCKLING HP/HT OF OFFSHORE STEEL PIPELINES

by
AIKATERINI AFENTOULI

Submitted in partial fulfillment of the requirements for the degree of Diploma in Mechanical Engineering at the University of Thessaly

Volos, 2021

Approved by the Committee on Final Examination:

Advisor	Dr. Spyros A. Karamanos, Professor, Department of Mechanical Engineering, University of Thessaly
Member	Dr. Panos Dakoulas, Professor, Department of Civil Engineering, University of Thessaly
Member	Dr. Michalis Agoras, Assistant Professor, Department of Mechanical Engineering, University of Thessaly

Date Approved: [July 09, 2021]

Acknowledgments

I would like to express my sincere thanks to the supervisor of my dissertation, Professor Mr. Spyros Karamanos, for his valuable help and guidance during the implementation of my work.

I am also grateful to the other members of the examination committee of my dissertation, Professors Mr. Michalis Agoras and Panos Dakoulas, for the careful reading of my work and their valuable suggestions.

I am thankful to Grigoris Sarvanis and Giorgos E. Varelis for their valuable help in modeling using the Abaqus program and their assistance in the Chapter 3 simulations. Finally, I thank my friends Vana, Katerina, and Eliza for their moral support and understanding, especially during the last months of my effort.

I am grateful to my parents, Despina and Fotis, and to my brother Haris for their wholehearted love and support all these years.

I dedicate this work to my best friend, Toby.

FINITE ELEMENT ANALYSIS OF LATERAL BUCKLING HP/HT OF OFFSHORE STEEL PIPELINES

AIKATERINI AFENTOULI

Department of Mechanical Engineering, University of Thessaly

Supervisor: Dr Spyros A. Karamanos

Professor of Structural Mechanics

Abstract

Offshore pipelines are used widely for the transportation of hydrocarbons or hot oils in great depths. They are of great economic importance, and a pipeline failure can lead to a considerable loss. The temperature variations due to the hot contents of the pipe can reach up to 180 ^{o}F (100 ^{o}C), and the pressure difference across the pipe wall can reach up to 1450 lb/in.^{2} (10 MPa). Under these two loading conditions, strong axial compressive forces are created that can lead to the pipeline's global or local buckling.

Offshore pipelines can be either buried or laid on top of the seabed. This thesis focuses on steel pipelines placed on the sea bed that are subjected to lateral buckling. These types of pipelines are usually partly embedded on the sea bed, thus making the resistance of the soil a critical design parameter in assessing the pipeline behavior. Lateral buckling can be used to control the behavior of the pipeline as long as it occurs in a controlled manner. In this thesis, finite element models are developed to assess these systems' behavior under high pressure and high-temperature conditions for various initial imperfections widths, internal pressures, and temperature values.

It was found that the maximum temperature that the pipe can withstand before buckling decreases as the initial imperfection width increases. Furthermore, the results show that reducing the initial imperfection length causes a significant reduction of the temperature that initiates the buckling response. On the contrary, the maximum temperature values increase with the increase of the pipeline thickness. In addition, the decrease of the pipeline's operating pressure also leads to a slight increase in the maximum temperature.

Key-words: buckling, lateral buckling HP/HT, finite element analysis, offshore pipelines

ΑΝΑΛΥΣΗ ΠΕΠΕΡΑΣΜΕΝΩΝ ΣΤΟΙΧΕΙΩΝ ΤΟΥ ΠΛΕΥΡΙΚΟΥ ΛΟΓΙΣΜΟΥ HP/HT ΥΠΟΘΑΛΑΣΣΙΩΝ ΑΓΩΓΩΝ ΑΠΟ ΧΑΛΥΒΑ

ΑΙΚΑΤΕΡΙΝΗ ΑΦΕΝΤΟΥΛΗ

Τμήμα Μηχανολόγων Μηχανικών, Πανεπιστήμιο Θεσσαλίας, 2021

Επιβλέπων Καθηγητής: Δρ. Σπύρος Α. Καραμάνος,
Καθηγητής Μηχανικής Κατασκευών

Περίληψη

Οι υποθαλάσσιοι αγωγοί χρησιμοποιούνται ευρέως για τη μεταφορά υδρογονανθράκων σε μεγάλα βάθη. Είναι μεγάλης οικονομικής σημασίας και η αστοχία του αγωγού μπορεί να οδηγήσει σε σημαντικές απώλειες. Οι διακυμάνσεις θερμοκρασίας λόγω του θερμού περιεχομένου του σωλήνα μπορεί να φτάσουν τους 180^{o} F (100^{o}C) και η διαφορά πίεσης στο τοίχωμα του σωλήνα μπορεί να φτάσει τα 1450 lb / $in.^{2}$ (10MPa). Κάτω από αυτές τις δύο συνθήκες φόρτισης, δημιουργούνται ισχυρές αξονικές θλιπτικές δυνάμεις που μπορούν να οδηγήσουν σε ολικό ή τοπικό λυγισμό του αγωγού.

Οι υποθαλάσσιοι αγωγοί μπορούν είτε να θάβονται είτε να τοποθετούνται πάνω στον βυθό. Αυτή η διπλωματική εργασία επικεντρώνεται σε αγωγούς από χάλυβα τοποθετημένους στον βυθό της θάλασσας οι υπόκεινται σε πλευρικό λυγισμό. Αυτοί οι τύποι αγωγών είναι συνήθως εν μέρει θαμμένοι στον πυθμένα της θάλασσας, καθιστώντας έτσι την αντίσταση του εδάφους μια σημαντική παράμετρο σχεδιασμού για την αξιολόγηση της συμπεριφοράς του αγωγού.

Ο πλευρικός λυγισμός μπορεί να χρησιμοποιηθεί για τον έλεγχο της συμπεριφοράς των αγωγών, εφόσον συμβαίνει υπό ελεγχόμενο τρόπο. Σε αυτήν την εργασία αναπτύσσονται μοντέλα πεπερασμένων στοιχείων για την αξιολόγηση της συμπεριφοράς αυτών των συστημάτων υπό συνθήκες υψηλής πίεσης και υψηλής θερμοκρασίας για διάφορα αρχικά πλάτη ατελειών, εσωτερικές πιέσεις και τιμές θερμοκρασίας.

Διαπιστώθηκε ότι η μέγιστη θερμοκρασία που μπορεί να αντέξει ο σωλήνας προτού λυγίσει μειώνεται καθώς αυξάνεται το αρχικό πλάτος της ατέλειας. Τα αποτελέσματα δείχνουν ότι, η μείωση του αρχικού μήκους της ατέλειας προκαλεί μεγάλη μείωση της θερμοκρασίας στην

οποία ξεκινά ο λυγισμός. Αντίθετα, οι μέγιστες τιμές θερμοκρασίας αυξάνονται με την αύξηση του πάχους του αγωγού. Η μείωση της πίεσης λειτουργίας του αγωγού οδηγεί επίσης σε μικρή αύξηση της μέγιστης θερμοκρασίας.

Λέξεις-κλειδιά: λυγισμός, πλευρικός λυγισμός HP / HT, ανάλυση πεπερασμένων στοιχείων, υποθαλάσσιοι αγωγοί

Contents

LIST OF TABLES

LIST OF FIGURES

Chapter 1. INTRODUCTION

1.1 Motivation

Offshore pipelines are subjected to several external loads. These loads can be in the form:

1. Internal or external pressure difference
2. Internal or external temperature difference
3. Residual stresses from laying
4. Weight of the pipeline and its contents
5. Buoyancy due to the surrounding seawater
6. Soil friction

For the pipeline to buckle, the pipe must be constrained in both ends so an axially compressive force will form. Otherwise, the pipeline will expand axially. Assuming that there are no residual stresses from the laying procedure, the axial force leading to the pipeline's eventual buckle is created mainly by the pressure and temperature changes on the pipe wall. For pipelines that deviate from straightness, these loads can render the pipeline unstable and result in local buckling. If the pipeline is laid on the seabed rather than buried, this phenomenon is called lateral buckling. These systems are typically embedded on the sea bed, which provides some initial resistance to the tendency of the pipe to move sideways when compressed axially and makes the soil resistance a crucial design parameter.

The axial resistance plays an essential role during the buckling of the pipeline. It affects the effective axial force responsible for buckling and the feed into lateral buckles. High axial resistance can reduce the feed-in but increases the axial force [1]. Axial soil resistance also has a vital role during each start-up and shut-down cycle of the pipeline. During start-up and shut-down, there is axial sliding between the pipe and the seabed [2].

The lateral resistance of the soil is difficult to predict due to its nature. For pipelines initially embedded on the sea bed, as they begin to move laterally, a berm of soil grows ahead of the pipe, creating additional resistance. The berm's size and strength increase until it

reaches a maximum value where the pipe “breaks through” and then stabilizes at a value called residual resistance [3].

The lateral buckling of offshore pipelines has been compared to that of railway tracks on a hot day. Railways, instead of buckling globally into a periodic mode shape, buckle locally near a pre-existing imperfection. Then, as the temperature rises, the adjacent track “feeds” into the growing buckles [4]. Thus, a long rail is a beam of small bending stiffness, and in order to sustain the load placed on it, it has to be supported along its length. This theory was later applied to many other situations as well. For example, a thin-walled cylindrical shell loaded by pressures that vary with the longitudinal direction but are constant circumferentially [5]. Because of that, offshore pipelines can generally be modeled as a beam on a rigid or elastic foundation.

The study of such systems is of utmost importance for the design and operation of pipelines. The design, placement, and operation of offshore pipelines is a costly and time-consuming procedure. They have to be designed to operate long-term and stay structurally safe even after a local buckle is present. The necessity of knowing the way these systems behave lies in the difficulty of replacing and repairing them due to the great depths at which they operate. In case of failures, such as a wall puncture or a fracture, the loss of production is substantial.

Lateral buckling does not affect the pipe’s integrity as long as it occurs in a controlled manner. Therefore, it can be used to control the behavior of the pipeline. Furthermore, periodic imperfections can be used to control the behavior of the pipeline and act as expansion loops [6]. The contribution of this thesis is that it studies the post-buckling behavior of pipelines that buckle laterally due to the presence of an initial imperfection. Finite element analyses are carried out for a range of initial imperfections, pipe thickness, and operating pressures.

1.2 Literature Review

There are several papers on upheaval buckling of offshore pipelines, but studies are limited on lateral buckling of pipelines.

The literature related to estimating the post-buckling behavior of offshore pipelines laid on top of the seabed is divided into three categories. The first category includes papers on the estimation and modeling of the pipe–soil interaction properties ([1], [2], [3], and [7]). The second category includes tasks that study the lateral buckling movement of the pipeline ([4],

[8], [9], [10], [11], and [12]). The third category focuses on the effect of pre-existing imperfections introduced to the pipeline through the Residual Curvature Method ([6], and [13]).

Roger E. Hobbs [10] studied the in-service buckling of heated pipelines. They found that horizontal snaking modes (or later buckling) occur at a lower axial load than vertical (upheaval buckling). They are therefore dominant unless lateral resistance is provided by trenching. Miles and Calladine [4] studied the post-buckling behavior of laterally buckled pipelines. They performed small-scale model testing and computer simulations to assess buckle lobes' growth and transfer to adjacent, newly formed lobes with a continuous temperature rise.

Many studies have shown the effect of pre-existing imperfections on the pipeline introduced through the Residual Curvature Method. Most recently, Weihan Zhang and Stelios Kyriakides [6] studied the effectiveness of periodic imperfections, which work as expansion loops for the pipeline. They concluded that the RCM is an efficient method of introducing those periodic geometric imperfections to a pipeline and can control lateral buckling of pipelines placed on a frictional sea bed.

Regarding the pipe–soil interaction estimation, Randolph, White, and Yan [2] have provided a theoretical framework for assessing the magnitude of axial friction during the start-up and shut-down period of a seabed pipeline. Also, White, Ganesan, and Bolton [7] have researched the axial resistance between seabed pipelines and fine-grained soils through a series of sweeps of a long plastic pipe over a bed of soft clay. They found that the peak value of the equivalent friction factor can reach as high as 1.5, and the residual values varied from 0.2 to 0.5. For a higher rate of movement, the residual values fell below 0.1. Finally, white and Dingle [3] concluded that the large-amplitude lateral pipe-soil resistance is not a 'frictional' response. Instead, it is governed predominantly by the passive resistance ahead of the pipe. Furthermore, that resistance is strongly influenced by the initial pipe embedment and any changes in the soil strength when remolded ahead of the pipe.

1.3 Thesis Organization

The rest of this thesis is organized into four sections occupying Chapters 2 – 5, respectively. Specifically:

In Chapter 2, the geometry of the pipeline and its material properties are introduced. Also, the model for the pipe-soil interaction and the types of imperfections to be used in the rest of the thesis are presented.

Chapter 3 gives an overview of the Abaqus program, presents how the problem was modeled and run through Abaqus, and describes the analyses carried out throughout this thesis.

In Chapter 4, all the numerical results of the Abaqus analyses are presented for various imperfection widths and lengths and different loads.

The final results and conclusions of this thesis and suggestions for further research are presented in Chapter 5.

Chapter 2. PROBLEM FORMULATION

In this chapter, the geometric characteristics of the pipe and its interaction with the ground are analyzed. Also, the type of initial imperfection used in this dissertation is presented.

2.1 Pipe Geometry

In a recent study by Zhang and Kyriakides [6], the overall length of the pipe was equal to L = 3922D. A similar relation for calculating the pipe's length was used in this thesis as well. The total length was calculated from Eq. (2.1) and is equal to 971.55, which was rounded up to 972 m. The pipe geometry data are summarized in Table 2.1.

$$L = 3000D_o \quad (2.1)$$

Pipe outer diameter D_o	12.75 in.
Pipe Thickness t	0.5 in.
Pipe Length L	972 m
D / t	25.5
L /D_o	3001.4

Table 2.1 Pipeline Geometric Properties

Because the problem is symmetrical about the axis that runs along its length (x-axis), only half the pipe's length was modeled to save computation time and memory. Thus, the half-pipe length is equal to 486 m.

2.2 Pipe Material

The selection of the pipe material is a crucial step during the design procedure of the pipeline. It has to withstand strong compressive loads and high temperatures and pressures during its operation period. According to the Safeback Design Guideline, the pipe material can be CMn steel up to X65. DNV-RP-F110 requires steel from the range X60 up to X70 [14].

In this thesis, the pipe material was assumed to have an elastic-plastic behavior and follow the material properties of X65 Steel which are given in Table 2.2. X65 is a high-level grade pipe used for onshore and offshore oil and gas transmission. In Figure 1, the Engineering Strain – Engineering Stress is plotted. The plastic strain – true stress curve is plotted in Figure 2. No outercoat for the pipeline was assumed. The effect of temperature on the material of the pipeline was not considered.

Steel Density ρ	7860 kg/m^3
Young's Modulus E	195 GPa
Specified minimum yield strength σ_y	553.4 MPa
Poisson's Ratio	0.3
Thermal Coefficient of Expansion	1.2E^{-05} 1/°C

Table 2.2 Steel Properties

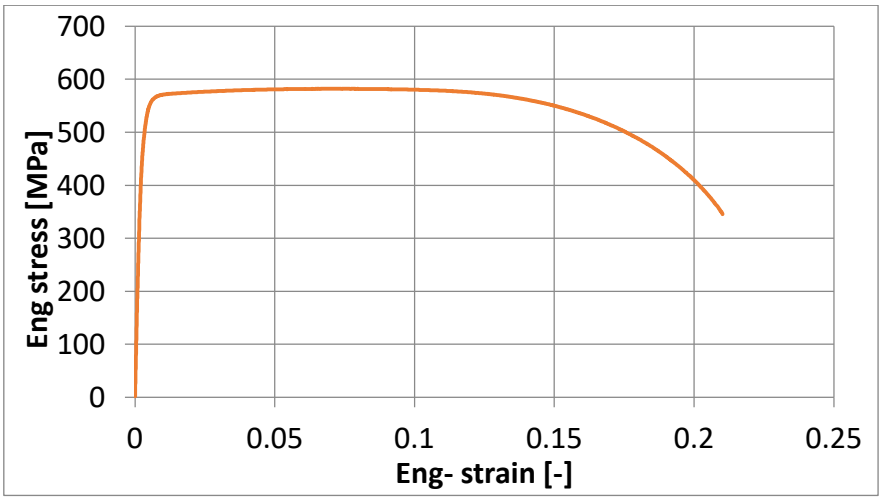

Figure 1: Engineering Strain - Engineering Stress Curve

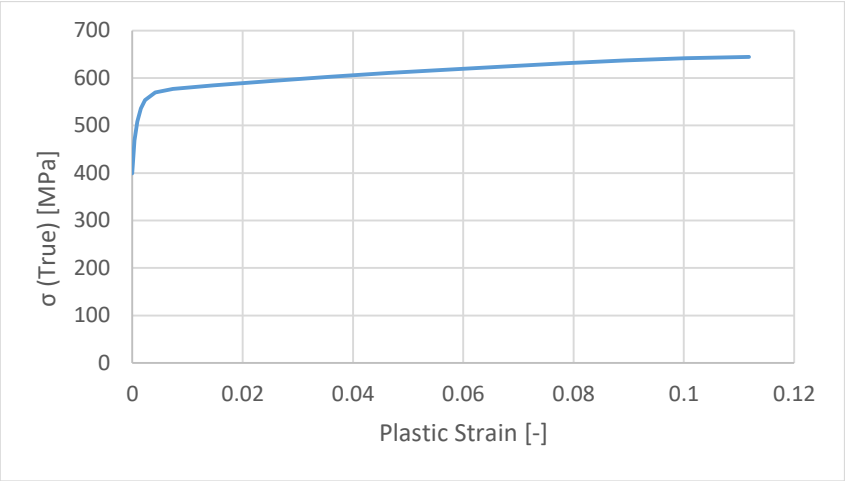

Figure 2: Plastic strain – True stress curve

Since it is some hydrocarbon, the density of the pipe's content will be much lower than that of the pipe. Therefore, it was assumed to be equal to 1 kg/m^3. The seawater was considered to have a density of 1000 kg/m^3.

Buoyancy due to the surrounding seawater causes a reduction in the total weight of the pipeline. To account for that weight change, the pipe's density that was used was 6865 kg/m^3, which produces the same weight per unit length as to if to subtract the water weight from the total pipe weight. This procedure was followed so that there is no need to define two distributed loads during the Abaqus analysis and does not affect the rest of the material properties.

2.3 Pipe – Soil Interaction

The behavior of the soil used in all the models of this thesis is presented in Figures 3 and 4 and was introduced by Seyfipour, Walker & Kimiaei [12].

In the lateral direction, the friction coefficient is assumed to reach its maximum value of 1 at 30 mm of lateral slip, decrease to 0.5 when the displacement is increased to 150 mm, and remain constant for further lateral movement of the pipe due to the growing berm of soil ahead of the pipe [3]. As the movement proceeds, the strength of soil within the berm is reduced, and sliding occurs at a lower resistance where the friction coefficient varies from 1 to 0.5. With the further displacement of the pipe, the friction coefficient remains constant at 0.5, assuming there is no reformation of the berm ahead of the pipe. The same behavior in tension and compression was assumed

In the axial direction, where movement is limited, the friction coefficient reaches its maximum value of 0.5 at a very small displacement of 5 mm and remains constant after. The same behavior in tension and compression was assumed

No friction model was needed in the vertical direction since the pipeline movement was restrained from moving upwards.

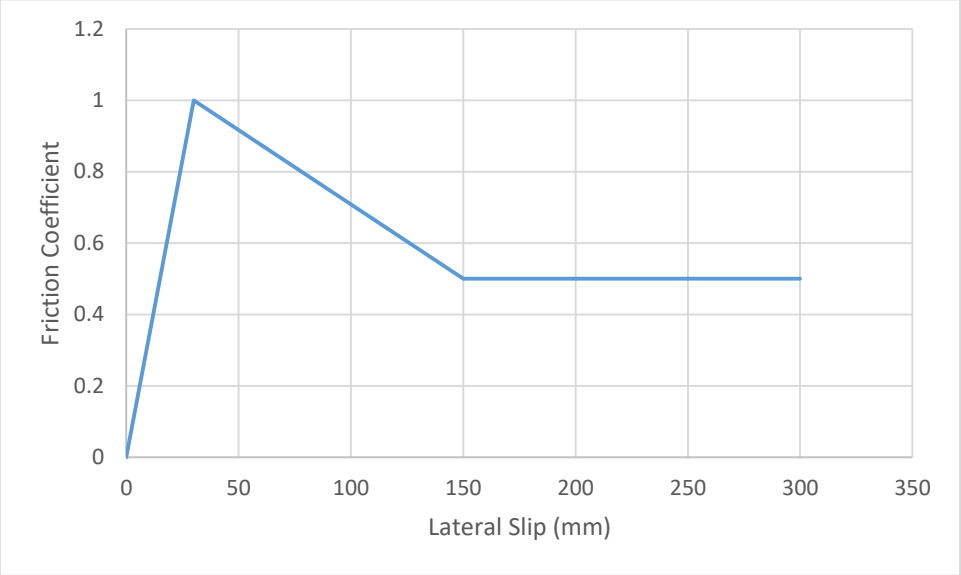

Figure 3: Pipe-soil interaction model in the lateral direction

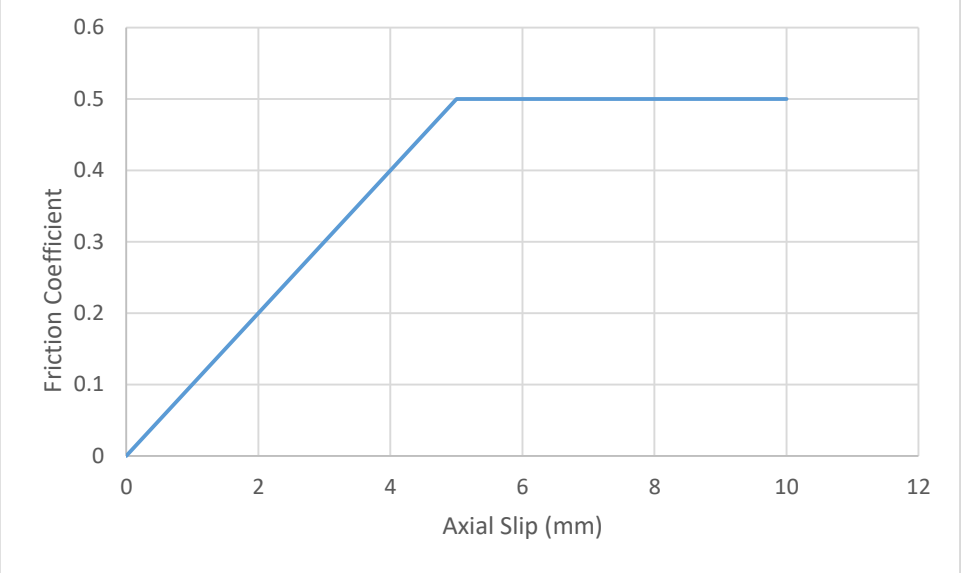

Figure 4: Pipe-soil interaction model in the axial direction

2.4 Imperfection

An imperfection on the pipeline's geometry can be introduced by an uneven sea bed, during the pipeline's laying process (Residual Curvature Method) [13] or due to a defect during the production phase of the pipeline.

A typical post-buckling shape of a pipeline laid on the seabed can be seen in Figure 5. The pipeline forms an S-shaped curve symmetrical about a point. This form resembles the movement of a snake hence why the phenomenon of lateral buckling is also called "Horizontal Snaking" [9].

The pipeline is assumed to be laid on an even seabed and has a localized geometric imperfection define by:

$$w_o = \begin{cases} f(x), & 0 \le |x| \le L_o, f(0) = \Delta_o \\ 0, & |x| > L_o \end{cases} \quad (2.2)$$

The imperfection is symmetric about $x = 0$ [8], [11]. Figure 6 shows the top-down view of a pipeline with the above type of imperfection.

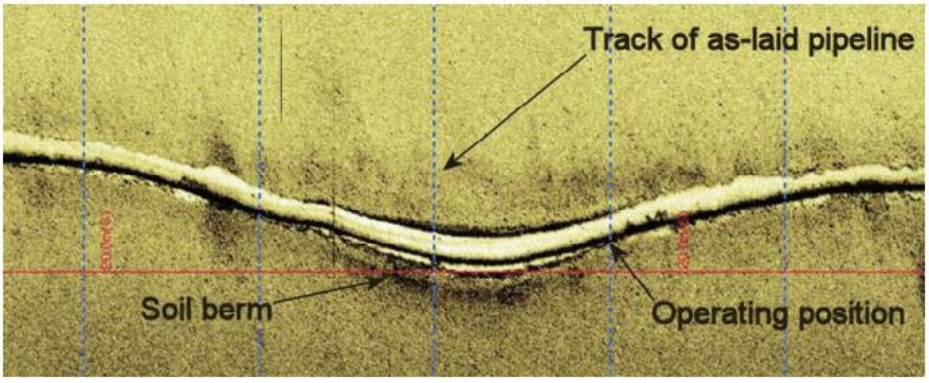

Figure 5: Post-buckling shape of the pipeline

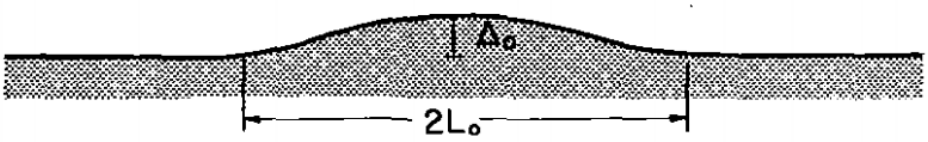

Figure 6: Top-down view of the assumed geometric imperfection shape

Two types of initial imperfections were examined. Both were introduced in (Thermal Buckling of Offshore Pipelines, Ju & Kyriakides). The first imperfection is a sinusoidal function and is given by the following expression:

$$f_1(x) = \frac{\Delta_o}{2}\left[1 + cos\frac{\pi x}{L_o}\right] \quad (2.3)$$

Figure 7 plots the second derivative of $f_1(x)$ for $\Delta_o = 0.5$ m and $L_o = 100$ m. As it can be seen, $f_1''(x)$ is discontinuous at $x = L_o$. Because of that, a different imperfection was considered. It was also introduced in (Thermal Buckling of Offshore Pipelines, Ju & Kyriakides) and had a much smoother finish at $x = L_o$. The second imperfection is a polynomial function and is given by the following expression:

$$f_2(x) = \Delta_o\left[\frac{8}{3}\left(\frac{x}{L_o}\right)^2 + 3\left(\frac{x}{L_o}\right) + 1\right]\left(1 - \frac{x}{L_o}\right)^3 \quad (2.4)$$

Since this thesis does not focus on examining the initial imperfection's shape influence to the resulting buckling, the second imperfection was used so that there was no possible interference of the non-continuity at $x = L_o$ with the resulting buckling behavior of the pipeline. In Figure 8, the second derivative of $f_2(x)$ is plotted for $\Delta_o = 0.5$ m and $L_o = 100$ m. In Figure 9, the imperfection shapes of $f_1(x)$ and $f_2(x)$ are plotted.

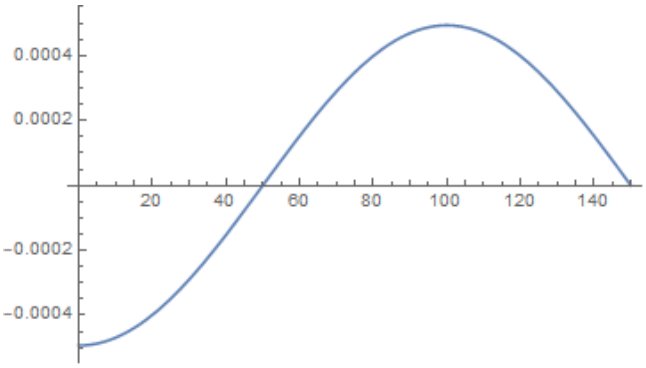

Figure 7: Second derivative of $f_1(x)$ for $\Delta_o = 0.5$ m and $L_o = 100$ m

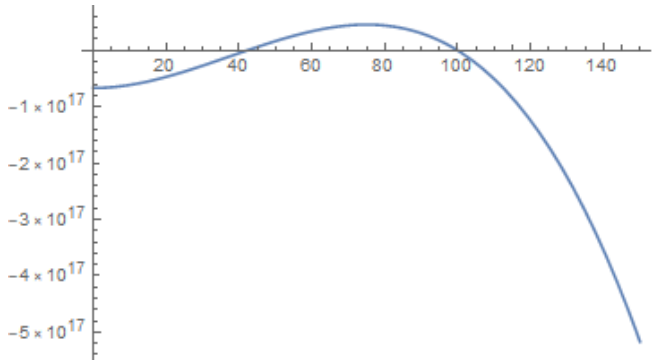

Figure 8: Second derivative of $f_2(x)$ for $\Delta_o = 0.5$ m and $L_o = 100$ m

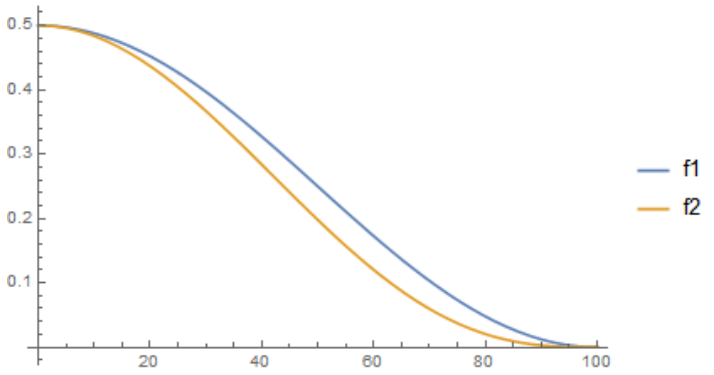

Figure 9: Comparison of imperfection shapes for $\Delta_o = 0.5$ m and $L_o = 100$ m

Chapter 3. FINITE ELEMENT ANALYSIS USING ABAQUS

In this chapter, the modeling of the problem on Abaqus and the analysis procedure that was followed is analyzed.

3.1 Abaqus Overview

Abaqus is an engineering modeling software for finite element analysis and computer-aided engineering developed by Dassault Systèmes. Abaqus/Standard employs solution technology ideal for static and low-speed dynamic events where highly accurate stress solutions are critically important. Abaqus/Standard is supported within the Abaqus/CAE modeling environment [15]. All model analyses in this thesis are carried out in Abaqus/Standard.

Abaqus has no built-in system of units. The units used in each model are decided by the user and have to be consistent throughout the analysis. In this thesis, the units that were used are presented in Table 3.1.

Quantity	**Unit**
Length	m
Force	kN
Mass	kg
Time	-
Stress	kPa
Energy	-
Density	kg / m^3

Table 3.1 Abaqus units

3.2 Elements

The whole pipeline section was modeled using ELBOW31 elements. Elbow elements are intended to accurately model the non-linear response of initially circular pipes and pipe bends when distortion of the cross-section by ovalization and warping dominates the behavior. They appear as beams but are shells with quite complex deformation patterns allowed and use plane stress theory to model the deformation through the pipe wall. However, they cannot provide nodal values of stress, strain, and other constitutive results. Element types ELBOW31 are one of the most complete elbow elements. In these elements, the ovalization of the pipe wall is made continuous from one element to the next, thus modeling such effects as the interaction between pipe bends (elbows) and adjacent straight segments of the pipeline [16].

Elbow elements contain, by default, five integration points along the pipe thickness, 20 integration points around the pipe, and 6 Fourier modes (Fig. 10). These default values were used in all models.

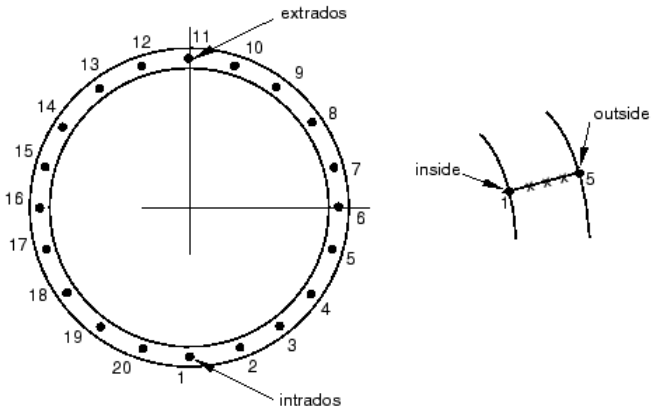

Figure 10: Elbow elements integration points around the pipe and thickness

All models in this thesis use ELBOW31 elements. Because elbow elements are not directly supported in Abaqus CAE, the input file had to be created manually and run through Abaqus Command-Line for each model using the command:

Abaqus job = file_name

3.3 Pipe Foundation Elements

For the soil, PSI34 elements were placed along the length of the pipe. PSI34 are three-dimensional pipe-soil interaction elements, and they are used to model the pipe's interaction with the surrounding soil. Through PSI elements, a non-linear reaction model can be defined with different behavior along the three axes. These elements have only displacement degrees of freedom at their nodes. One side or edge of the element shares nodes with the underlying pipe or elbow element that models the pipeline. The nodes on the other edge represent a far-field surface, such as the ground surface [16]. Therefore, care must be taken when connecting the PSI elements to the adjacent ELBOW element.

For the pipe-soil interaction model to be assigned to the elements, the following option is used:

* PIPE-SOIL INTERACTION, ELSET=name
*PIPE-SOIL STIFFNESS, DIRECTION=direction, TYPE=NONLINEAR
Force per unit length along pipeline, Relative displacement

ELSET denotes the element set on which the stiffness will be applied. The DIRECTION parameter states the direction of the stiffness, and the TYPE parameter is used to declare the non-linear behavior of the surrounding soil. The data line is repeated as many times as required to define the interaction model [17].

For the pipe-soil interaction model to be assigned to the elements, the force per unit length and the corresponding displacement along each direction must be specified. The is calculated in kN / m using the relation:

$$W_L = \rho V_L g \cdot 10^{-3} \left(\frac{kN}{m}\right) \quad (3.1)$$

$$F = \mu \cdot W_L \left(\frac{kN}{m}\right) \quad (3.2)$$

W_L is the pipe's weight per unit length, and V is the pipe's volume per unit length calculated from Eq. (3.3). The input file configuration is shown in Figure 11.

$$V_L = \frac{\pi}{4}(D_{out}^2 - D_{in}^2)\ (m^2) \quad (3.3)$$

```
*PIPE-SOIL INTERACTION,ELSET=SOIL
*PIPE-SOIL STIFFNESS,DIRECTION=AXIAL,TYPE=NONLINEAR
-0.478615428,-0.005
0,0
0.478615428,0.005
*PIPE-SOIL STIFFNESS,DIRECTION=VERTICAL,TYPE=NONLINEAR
0,-0.015
0,0
0,0.015
*PIPE-SOIL STIFFNESS,DIRECTION=HORIZONTAL,TYPE=NONLINEAR
-0.478615428,-0.15
-0.957230856,-0.03
0,0
0.957230856,0.03
0.478615428,0.15
```

Figure 11: Pipe-soil interaction model definition in the input file

3.4 Imperfection

The imperfection was introduced to the model through the input file key-word *IMPERFECTION. This option is used to introduce a geometric imperfection into a model for a post-buckling analysis.

The input file key-word had the following form:

*IMPERFECTION, INPUT=name

Where: the INPUT parameter is equal to the name of the file consists of lines containing the imperfection per node in the form of Node number, imperfection in the first coordinate direction, imperfection in the second coordinate direction, imperfection in the third coordinate direction[17].

To produce the file, the coordinates of the nodes along with the node numbers were imported in an excel sheet, and the corresponding displacement in the z-direction was calculated from the imperfection equation (Eq. (2.4)). Then, those numbers were converted to a comma-separated txt file with the format mentioned above.

3.5 Mesh

For all the models, a mesh that was denser near the imperfection's center and sparser as it moved along the length of the pipe was used. The element width and the element number per segment are given in Table 3.2. This led to reduced running times and smaller data files. Also, the accuracy of the results near the imperfections half-length was not affected.

Segment	Element Width	Number of elements
0D - 100D	0.0295	1121
100D - 250D	0.0608	791
250D - 1500D	0.1215	3333

Table 3.2 Abaqus element sizes

To generate the mesh, first, the two outmost nodes of the pipe were created with *NODE, and the rest were generated incrementally through the command *NGEN, which are formatted as follows in the input file:

*NODE
Node number, 1st coord, 2nd coord, 3rd coord
*NGEN, NSET=name
Number of the first end node, Number of the second end node, increment in the numbers between each node along the line

Where NSET is equal to the name of the node-set containing the corresponding nodes [17]. As mentioned previously, only the half-pipe length is modeled to cut down on analysis time and memory. The above input file configuration for generating the ELBOW and PSI nodes is shown in Figure 12.

```
*NODE
1       ,       0       ,       0       ,       0
1122    ,       33      ,       0       ,       0
1914    ,       81      ,       0       ,       0
5248    ,       486     ,       0       ,       0
*NGEN, NSET=N01
1   , 1122  , 1
*NGEN, NSET=N02
1122   , 1914  , 1
*NGEN, NSET=N03
1914   , 5248  , 1
```

(a)

```
*NODE
100001   ,       0       ,       -2      ,       0
101122   ,       33      ,       -2      ,       0
101914   ,       81      ,       -2      ,       0
105248   ,       486     ,       -2      ,       0
*NGEN, NSET=NS1
100001   , 101122  , 1
*NGEN, NSET=NS2
101122   , 101914  , 1
*NGEN, NSET=NS3
101914   , 105248  , 1
```

(b)

Figure 12: Input file structure for generating (a) pipe nodes (b) soil nodes

The mesh was generated through the *ELGEN command in the input file. For the command to work, the first element of the part has to be created. The command is written as follows:

*ELEMENT, TYPE=element-type, ELSET=name
Element number
First node number forming the element
Second node number forming the element

The TYPE parameter is set equal to the name of the element used in the model (ELBOW31 or PSI34) and ELSET is equal to the name of the element set containing the corresponding elements.

*ELGEN, ELSET=name
Master element number

Number of elements to be defined in the first row generated, including the master element.
Increment in node numbers of corresponding nodes from element to element in the row
Increment in element numbers in the row
Number of rows to be defined, including the master row
Increment in node numbers of corresponding nodes from row to row
Increment in element numbers of corresponding elements from row to row

Where: ELSET is equal to the name of the node-set containing the corresponding elements [17]. The above input file configuration for generating the ELBOW and PSI elements is shown in Figure 13. In Figure 14, the half-pipe length along with the local coordinate system is shown. Also, in Figure 15, the distinction between the elements of the pipeline and the elements of the soil is made.

```
*ELEMENT, TYPE=ELBOW31, ELSET=PIPE01
1, 1, 2
*ELGEN, ELSET=PIPE01
1,1,1,1,5247,1,1
```

(a)

```
*ELEMENT, TYPE=PSI34, ELSET=SOIL
100001, 1,2, 100002,100001
*ELGEN, ELSET=SOIL
100001,1,1,1,5247,1,1
```

(b)

Figure 13: Input file structure for generating (a) pipe elements (b) soil elements

(a)

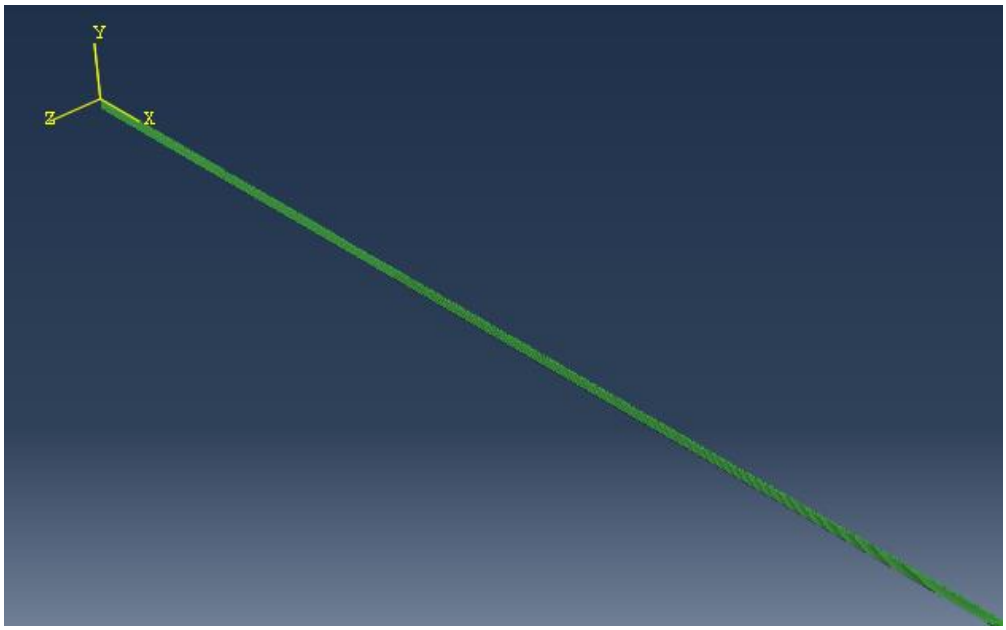

(b)

Figure 14: (a) Abaqus part instance, x-y plane (b) Local coordinate system

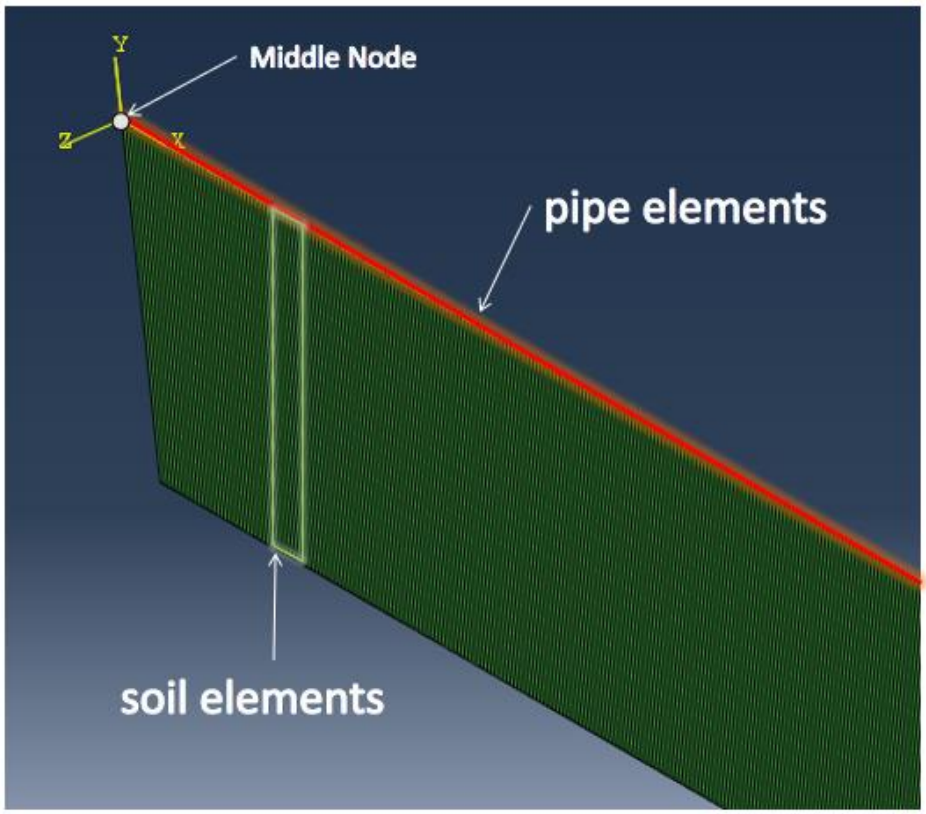

Figure 15: Pipe and soil elements on Abaqus part instance

3.6 Boundary Conditions

A fixed boundary condition was specified on each node of the PSI34 elements far-field surface. In addition, the following boundary conditions were applied to the right end of the pipe:

$$u_x = u_y = u_z = 0$$

On the far left node, an XSYMM condition was applied since only the half-pipe length was modeled.

In addition, $u_y = 0$ was applied to all pipe nodes to limit the movement only in the x-z plane and restrain the pipe from buckling upwards. Also, the pipe nodes were restrained from rotating in the x and z-direction: $\varphi_x = \varphi_z = 0$.

The boundary conditions were specified in the input file through the *BOUNDARY key-word [17]:

*BOUNDARY
Node or node set, first degree of freedom, last degree of freedom

All boundary conditions specified here are propagated to the steps that follow, and all of them stay active throughout the analysis, as shown in the Abaqus boundary condition manager in Figure 16. The above input file configuration for the boundary conditions is shown in Figure 17. The numbers shown correspond to the following degrees of freedom:

1: x-displacement
2: y-displacement
3: z-displacement
4: rotation about the x-axis
5: rotation about the y-axis
6: rotation about the z-axis
XSYMM: symmetry about a plane (x = constant, degrees of freedom 1, 5, 6 = 0)

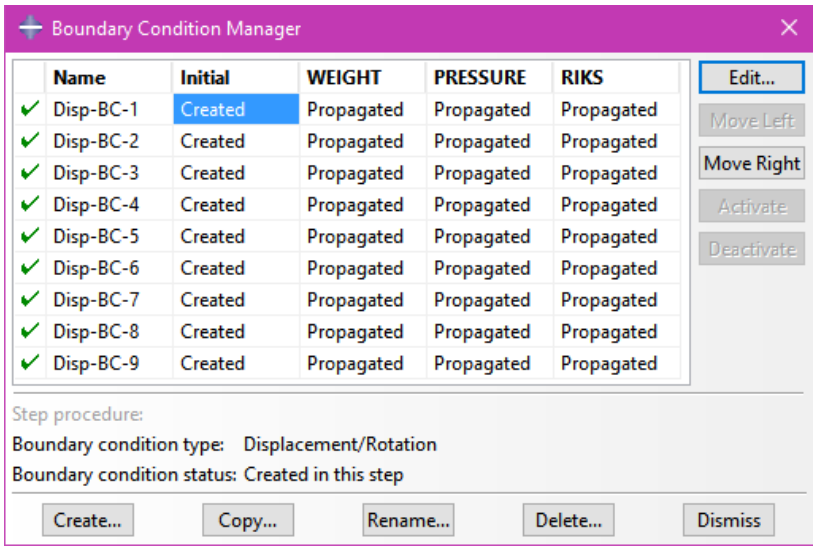

Figure 16: Abaqus boundary condition manager

```
*BOUNDARY
FIX   , 1, 3
RNODE,1,3
RNODE,4,4
RNODE,6,6
LNODE,XSYMM
LNODE_SOIL, XSYMM
PIPEN,2
PIPEN,4,4
PIPEN,6,6
```

Figure 17: Input file structure for specifying the boundary conditions

3.7 Initial Conditions

The initial temperature is specified as an initial condition. The difference between this initial temperature value and any later defined temperature fields will create thermal strains considering a thermal coefficient has been provided as a material property [17].

For the initial conditions, the initial temperature was set at $0^{o}C$ for all pipe nodes in the input file as follows:

*INITIAL CONDITIONS, TYPE=TEMPERATURE

Node set or node number, first initial temperature value at the node or node set.

Figure 18 shows the input file configuration and the Abaqus predefined temperature field window.

```
*INITIAL CONDITIONS,TYPE=TEMPERATURE
PIPEN,0
```

(a)

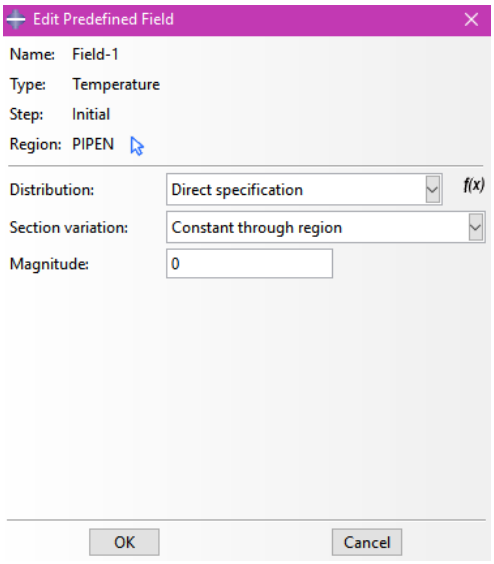

(b)

Figure 18: (a) Input file configuration for defining initial conditions (b) Abaqus predefined temperature field window

3.8 Analysis

The analysis begins with the placement of the total weight of the pipeline. Then, the internal pressure of the pipe was specified. The internal pressure that was set in this step is assumed to be the net pressure acting on the pipeline. Thus, no external pressure was defined. Following that, a Riks analysis was carried out with a temperature load of 100^{o}C.

3.8.1 Static Steps

The first two steps used to define the weight and the internal pressure are both static analysis steps. Because the problem includes an initial imperfection that introduces a non-linearity in the problem, a non-linear static analysis was performed. Abaqus/Standard uses

Newton's method to solve the non-linear equilibrium equations, and the solution is obtained as a series of increments. The increment size is of great importance. Newton's method has a finite radius of convergence; a large increment can prevent the algorithm from converging because the initial state is too far from the equilibrium state that is being sought [16]. Figure 19 shows the incrementation scheme used. However, the default automatic incrementation was not suitable for this analysis. Because these types of problems tend to render the model unstable and terminate the analysis prematurely due to convergence, issues control parameters were used. Solution control parameters are used to define tolerances for field equations.

To avoid premature cutbacks in complex analyses, it is useful to set $I_o = 8$ and $I_R = 10$. I_o is the number of equilibrium iterations after which the check is made that the residuals are not increasing in two consecutive iterations. The default value is four, but it was necessary to increase this value. I_R is the number of equilibrium iteration after which the logarithmic rate of convergence check begins. The default value is eight, but a higher value was needed [16]. These two changes were done by the following key-word in the input file:

*CONTROLS, ANALYSIS = DISCONTINUOUS

Also, tolerances for the moment field equations were defined with the following key-word:

*CONTROLS, PARAMETERS = FIELD, FIELD = field

Where the field parameter was set equal to ROTATION and the tolerance of the Moment Field Equations was set to 0.1 [17]. Figure 19 shows the input file structure for defining the weight and pressure steps.

```
*STEP, INC=99999, NLGEOM, UNSYMM=YES
Apply Weight
*STATIC
0.1, 1.0 , 1e-15, 0.5
*CONTROLS, ANALYSIS=DISCONTINUOUS
*CONTROLS, PARAMETERS=FIELD, FIELD=GLOBAL
1E-1,
*DLOAD, OP=new
PIPE, BY, -67.34565
```

(a)

```
*STEP, NAME=PRESSURE, NLGEOM=YES
Apply Pressure
*STATIC
0.01,1.,1E-15,1
*CONTROLS, ANALYSIS=DISCONTINUOUS
*CONTROLS, PARAMETERS=FIELD, FIELD=ROTATION
,1e-1
*Dload
PIPE, PI, 10000., 0.298450597
```

(b)

Figure 19: Static step windows: (a) Weight Static Step (b) Pressure Static Step

The loads that can be prescribed in a static stress analysis are concentrated nodal forces, distributed pressure, or body forces. For the weight, a distributed load per cubic meter is specified in the negative y-direction. For the pressure, the load type IP was selected (Internal Pressure), and the effective diameter was entered. Figures 20 and 21 show the load definition window and the force applied on the pipe nodes for the weight and pressure loads.

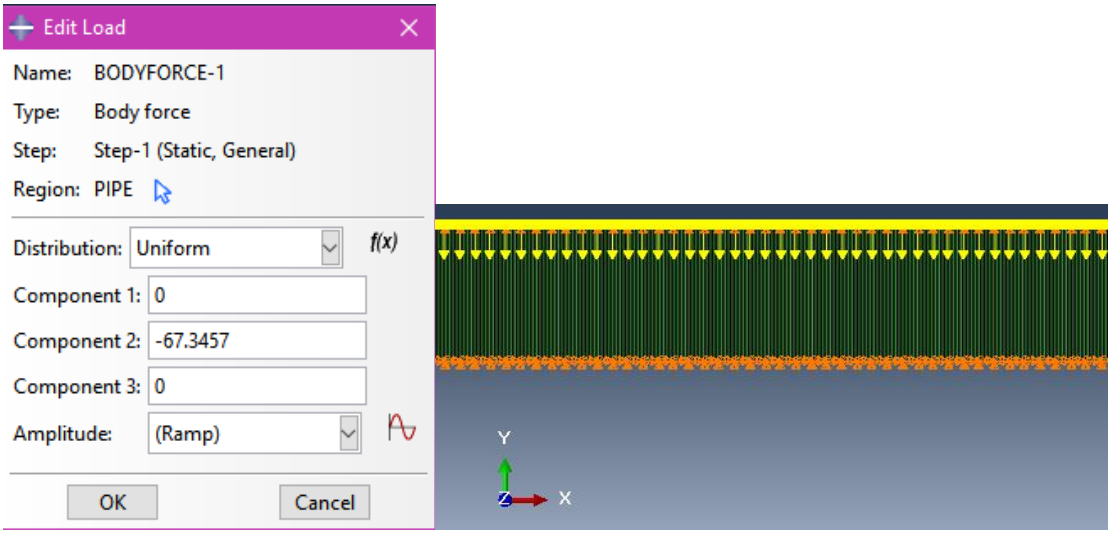

Figure 20: (a) Weight definition window (b) Weight force on pipe nodes

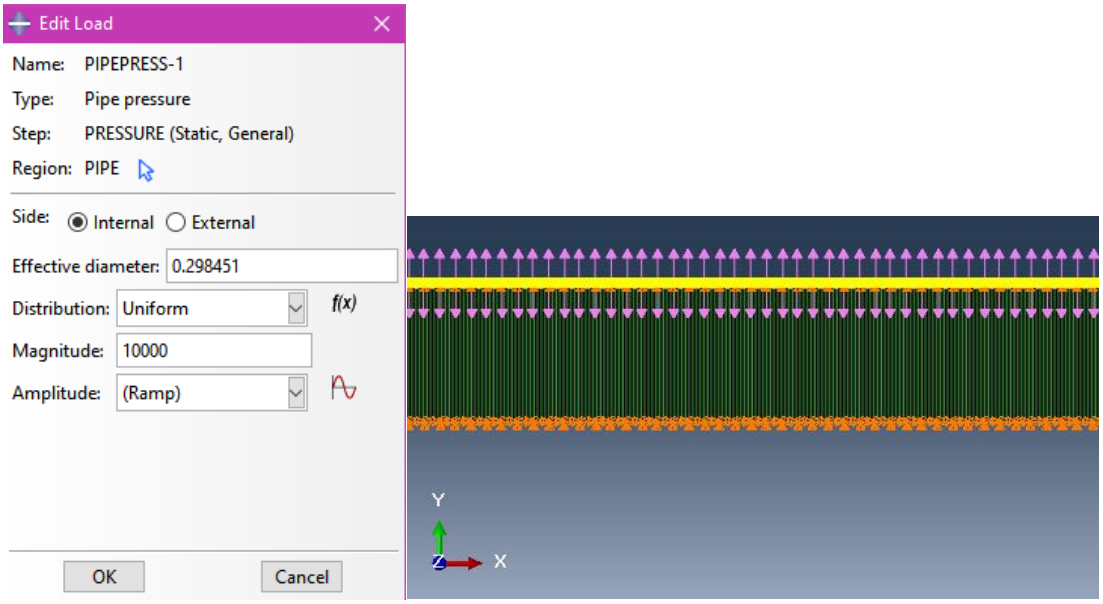

Figure 21: (a) Internal pressure definition windows (b) Internal pressure on pipe nodes

3.8.2 Riks Analysis

There are several approaches when modeling a non-linear static problem that involves post-buckling behavior. In this thesis, the analysis was done using the "modified Riks method." This method is used when the load magnitudes are governed by a single parameter, where the load is proportional. In a Riks analysis, the load is considered an extra parameter; and the algorithm solves simultaneously for loads and displacements.

The loads defined in previous steps are considered "dead" loads and are kept constant during this step. Therefore, only the load defined in a Riks step, the "reference" load, is used. To calculate the load's magnitude at a specific moment during the analysis, Eq. (3.4) is used.

$$Pt = P_o + \lambda\left(P_{ref} - P_o\right) \quad (3.4)$$

Where P_o is the "dead load', P_{ref} is the "reference load," and λ is the "load proportionality factor." From now, on the load proportionality factor will be shortened to LPF. Abaqus prints the value of LPF per increment. Since no previous temperature load was defined, P_o is equal to zero, and Eq.(3.8.1) reduces to:

$$Pt = \lambda P_{ref} \quad (3.5)$$

Eq. (3.5) is used to calculate the total temperature load per increment of the Riks analysis.

Abaqus/Standard uses Newton's Method to solve the non-linear equilibrium equations. The user provides the initial, minimum, and maximum increment sizes. The increment sizes were kept low to produce a smoother 'finish' in the charts created later. There two ways to specify when the Riks analysis will end. Either by selecting the maximum LPF or the maximum displacement value at a specified degree of freedom. If neither of these conditions is specified, the analysis will terminate when the maximum number of increments is reached [16]. No *CONTROL parameters were needed in this step. In Figure 22, the input file structure for defining the Riks step, the increment sizes, and the pipe nodes' temperature load is shown. The elapsed time varied from 9 – 12 hours per model.

```
*STEP, NAME=RIKS, NLGEOM=YES, INC=500
Riks - Temperature
*STATIC,RIKS
0.001, 1., 1e-15, 0.01, ,
*Temperature
PIPEN, 100
```

Figure 22: Riks step specification and temperature load definition

Chapter 4. NUMERICAL RESULTS

In this chapter, the numerical results from the Abaqus finite element analyses are presented. Specifically, we consider the influence of initial imperfection width and length, the pipeline thickness, and the internal pressure on the load proportionality factor, the pipe's displacement, and the reaction forces on the middle and end node of the pipeline.

4.1 Influence of initial imperfection width

We first consider the influence of the initial imperfection width on the pipe's displacement and deformation. The following imperfection widths were tested: Δ_o = 0.5, 0.6, 0.7, 0.8, 0.9, 1.2, and 1.6, for a constant imperfection half-length of L_o = 100 m and a constant internal pressure of 10 MPa.

The indication that the pipeline has begun to buckle locally is usually determined by a sudden drop of the effective axial load until it reaches a value from where it stays constant while the pipeline continues to buckle. In our case, the load which is applied incrementally is a temperature load. Because of the nature of the load, there is a sudden drop initially, and the load continues to grow and increase as the analysis continues. Thus, the force with which the pipeline's behavior is assessed is either the reaction force at the end or the center of the pipeline.

Figure 31 shows the load proportionality factor (or LPF) multiplied by the reference load versus the total displacement of the pipeline node that exhibits the maximum spatial displacement. As mentioned before, the temperature load per increment is calculated from Eq. (3.5):

$$Pt = \lambda P_{ref}$$

Here $P_{ref} = 100^0 C$, and the load proportionality factor λ per increment is extracted from the .odb file through Abaqus / CAE. There is a drop in the maximum temperature load that leads to the pipe's buckle. It decreases gradually as the initial imperfections width is increased.

The maximum temperature loads for each model are given in Table 4.1 and are plotted in Figure 34.

In Figure 30, a sketch of the pipeline imperfection and the reaction forces acting on its ends are drawn. RF_{END} is the reaction force acting on the pipline's end node and RF_{MIDDLE} the reaction force acting on the middle node of the pipeline. Figures 32 and 33 show the reaction forces on the center of symmetry and the end of the pipeline versus the maximum displacement along the pipe's half-length. It is evident that these forces behave the same way and are almost equal in value, differing only by a few kNs. As the width of the initial imperfection Δ_o increases, both the resulting reaction forces increase.

Figures 23 to 29 show a top-down view of the shape of the pipeline at the point of the analysis where the maximum lateral displacement is equal to 0.3 m. The red color shows the displacement of each node, and the blue color is the initial shape of the pipeline before the analysis begins. While in all the models, the maximum displacement is on the center of the pipeline, where the initial imperfection's width is the maximum, for 0.5 m, the maximum displacement is found about 74 m to the left of the middle node.

The weight does not produce any lateral movement to the pipe nodes. However, with the introduction of the internal pressure, the middle node's lateral displacement increases slightly. Furthermore, as the temperature starts to rise, its displacement increases to ≈ 0.03 m before it falls to ≈ 0.012 m, where it stays constant while the buckle grows on a different part of the pipeline. This behavior could be attributed to possible interference with the soil, which leads to a non-uniform resistance along the pipe. This resistance is responsible for the growth of the buckle at a different region from the rest of the models.

For the rest of the models, the internal pressure increases the displacement of the middle node, and the increase of temperature leads the buckle to be formed at the center of the pipeline.

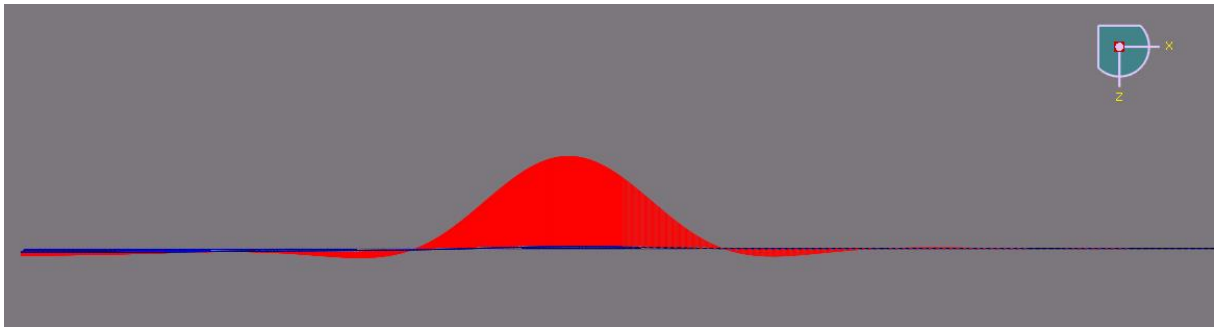

Figure 23: L_o = 100 m, Δ_o = 0.5 m, U_{MAX} = 0.3 m

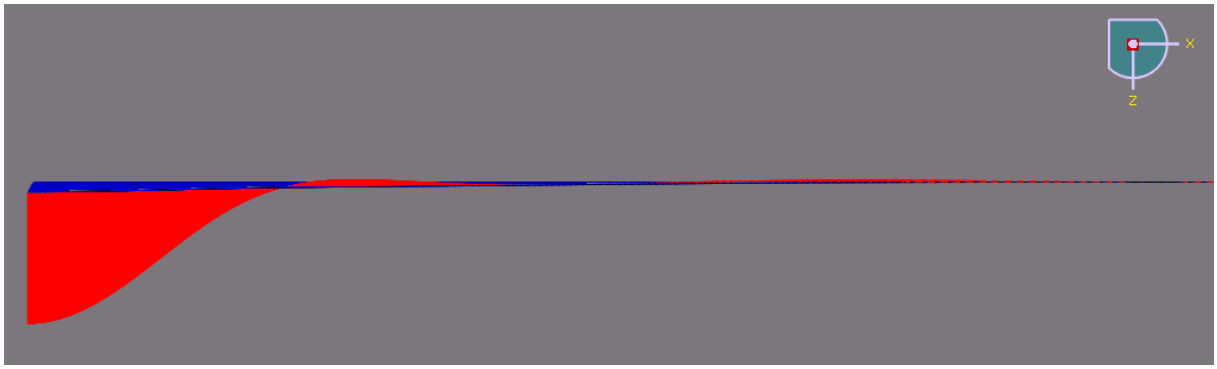

Figure 24: L_o = 100 m, Δ_o = 0.6 m, U_{MAX} = 0.3 m

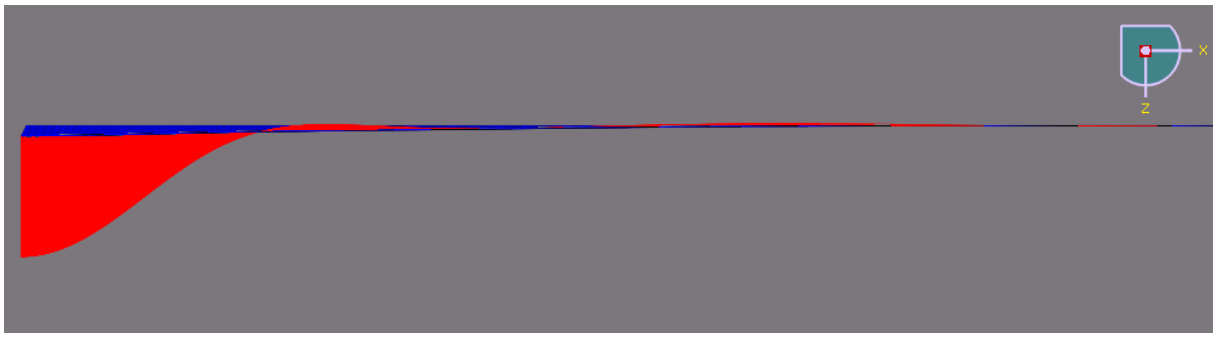

Figure 25: L_o = 100 m, Δ_o = 0.7 m, U_{MAX} = 0.3 m

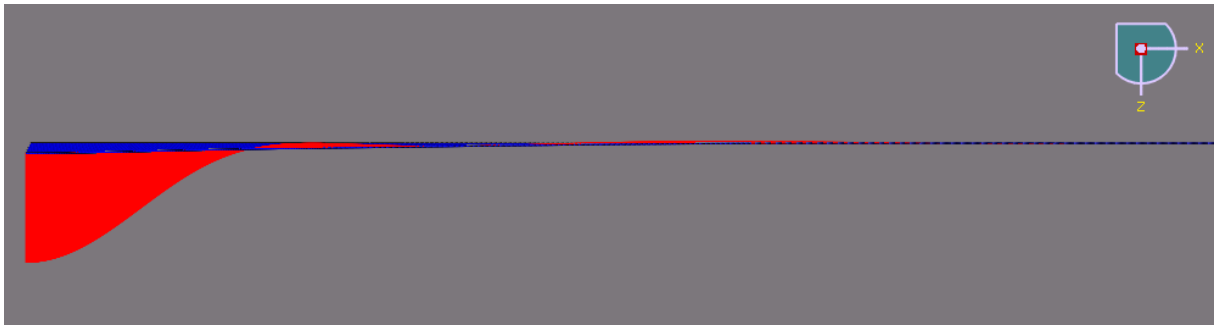

Figure 26: L_o = 100 m, Δ_o = 0.8 m, U_{MAX} = 0.3 m

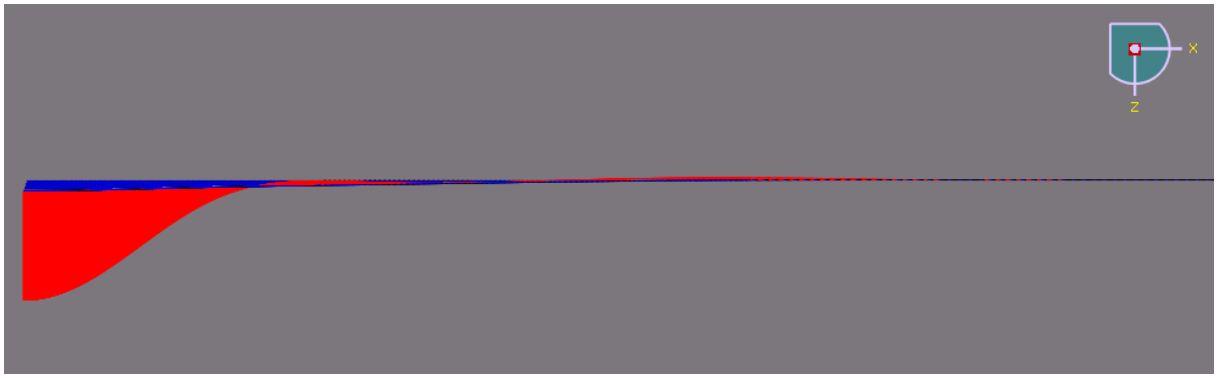

Figure 27: L_o = 100 m, Δ_o = 0.9 m, U_{MAX} = 0.3 m

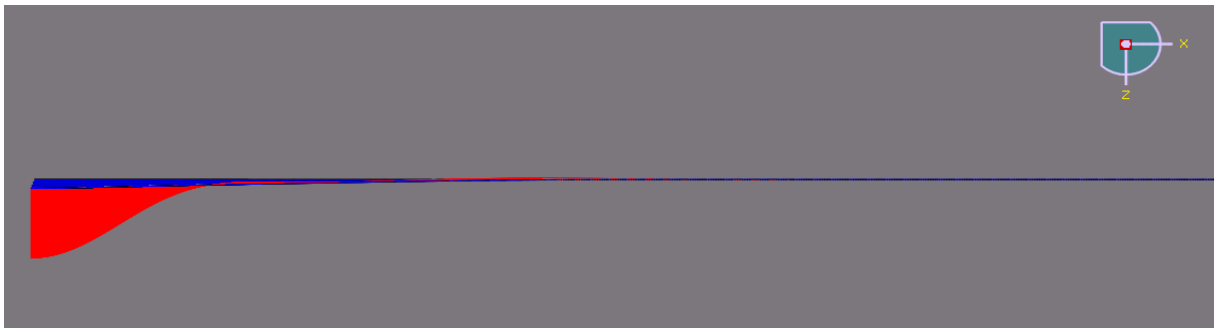

Figure 28: L_o = 100 m, Δ_o = 1.2 m, U_{MAX} = 0.3 m

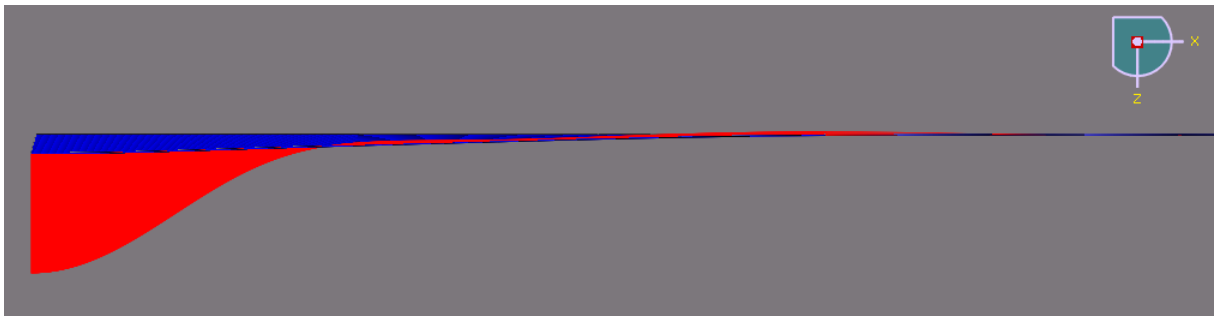

Figure 29: L_o = 100 m, Δ_o = 1.6 m, U_{MAX} = 0.3 m

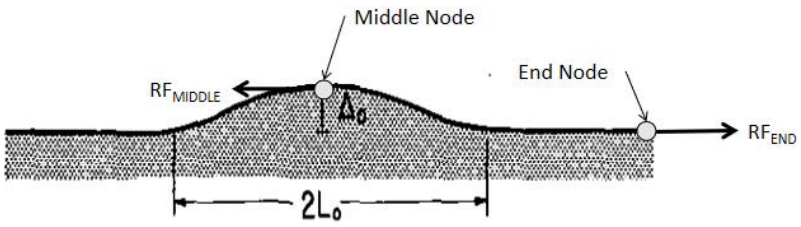

Figure 30: Reaction Forces Notation

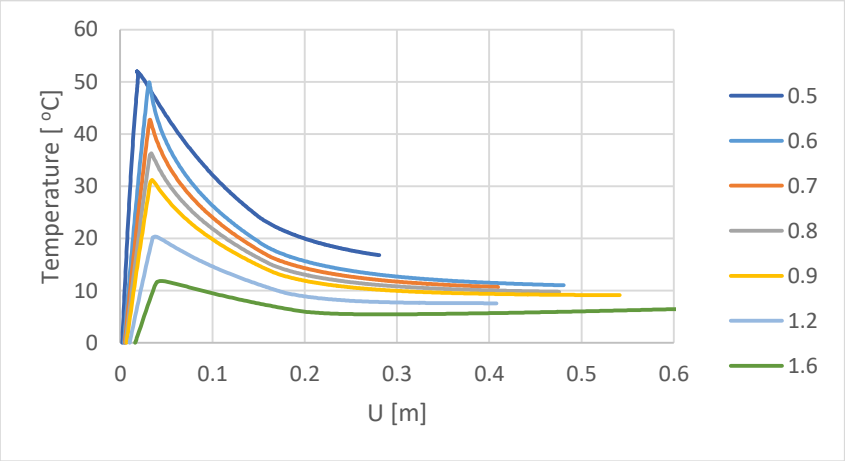

Figure 31: Temperature vs. Displacement for L_o = 100 m, p = 10 MPa, t = 0.5 in.

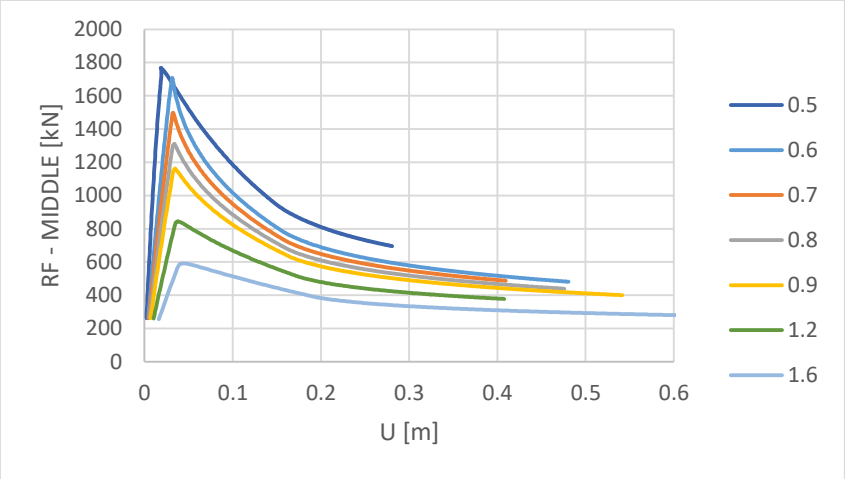

Figure 32: RF_{MIDDLE} vs. Displacement for L_o = 100 m, p = 10 MPa, t = 0.5 in.

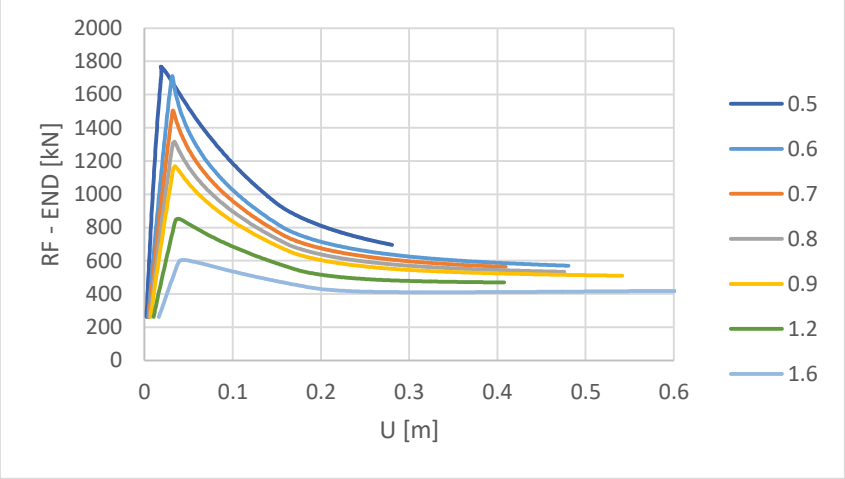

Figure 33: RF_{END} vs. Displacement for L_o = 100 m, p = 10 MPa, t = 0.5 in.

Δ_o [m]	Maximum Temperature Load [^oC]
0.5	51.987
0.6	49.922
0.7	42.746
0.8	35.954
0.9	31.235
1.2	20.382
1.6	11.840

Table 4.1 Maximum temperature loads per width of initial imperfection

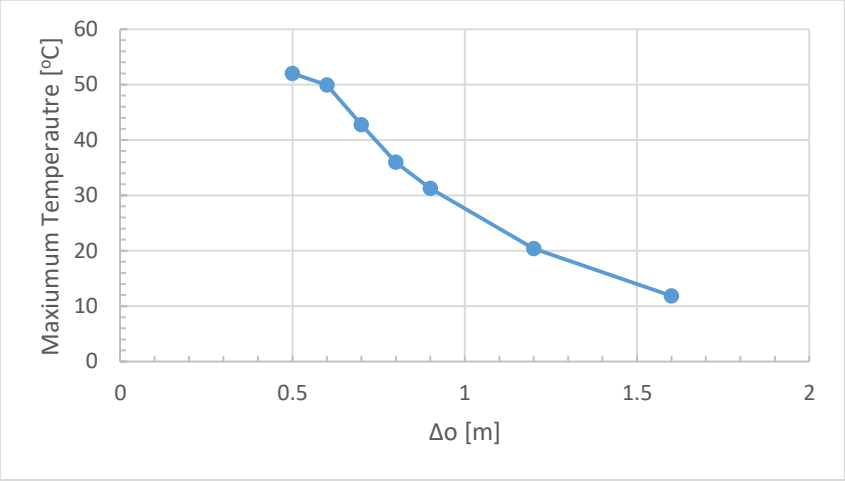

Figure 34: Maximum Temperature vs. Initial imperfection width Δ_o

4.2 Influence of initial imperfection length

Next, the influence of the initial imperfection length was considered. The following imperfection lengths were tested: L_o = 50, 75 and 100 m, for Δ_o = 0.5, and 0.9 m and constant internal pressure of 10 MPa.

The top-down view of the pipes' form when the maximum lateral displacement reaches 0.3 m is shown in Figures 35 to 38 for both L_o = 50 and 75 m. The red color shows the displacement of each node, and the blue color is the initial shape of the pipeline before the analysis begins. For an imperfection length of 50 m, the pipe begins to buckle at the center of the pipe where the imperfection is placed initially for both 0.5 and 0.9 m of imperfection

width, contrary to the results of section 4.1, where for a width of 0.5 m, the buckle initiates 74 m left of the pipe's middle node. For L_o = 75 m, the behavior is similar.

As in section 4.1, Figures 39 and 42 show the temperature load versus the total displacement of the node with the maximum spatial displacement for L_o = 50 and 75 m. The same behavior is observed; with the increase of the imperfection width, the pipeline's maximum load can withstand before buckling decreases. Here, the steady increase of the temperature load even after the buckle of the pipeline has begun is more clearly seen. The two curves increase and follow the same trajectory. The maximum temperature loads for each model are given in Table 4.2 and Table 4.3.

Figures 40, 41, and 43, 44 show the reaction forces on the center of symmetry and the end of the pipeline versus the maximum displacement along the pipe's half-length for L_o = 50 m and L_o = 75 m, respectively. The forces behave similarly as in section 4.1. As the width of the initial imperfection Δ_o increases, both the resulting reaction forces increase, fall, and stabilize about a constant value. However, for an initial length of L_o = 50 m, the reaction forces at the center of the pipeline, after the initial drop, increase slightly and stabilize at a constant value.

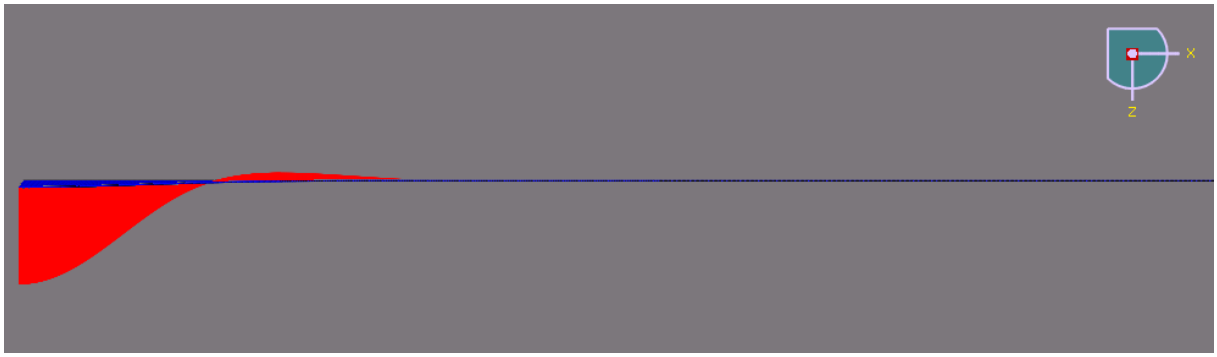

Figure 35: 10 MPa, L_o = 50 m, Δ_o = 0.5 m, U_{MAX} = 0.3 m

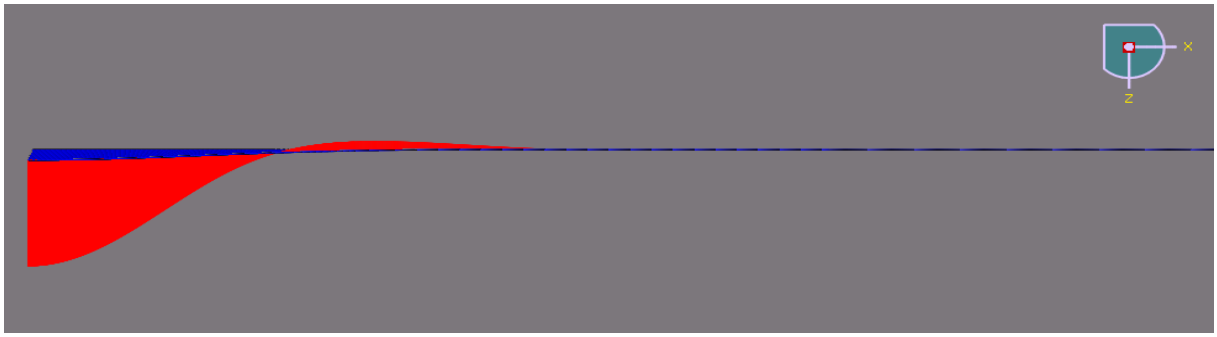

Figure 36: 10 MPa, L_o = 50 m, Δ_o = 0.9 m, U_{MAX} = 0.3 m

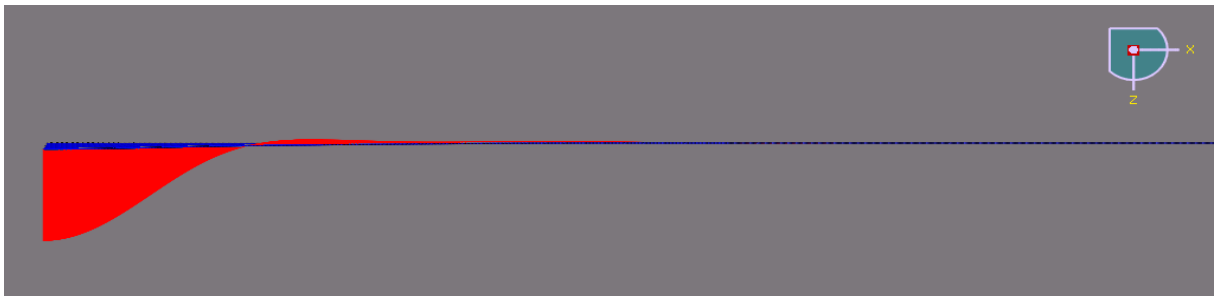

Figure 37: 10 MPa, L_o = 75 m, Δ_o = 0.5 m, U_{MAX} = 0.3 m

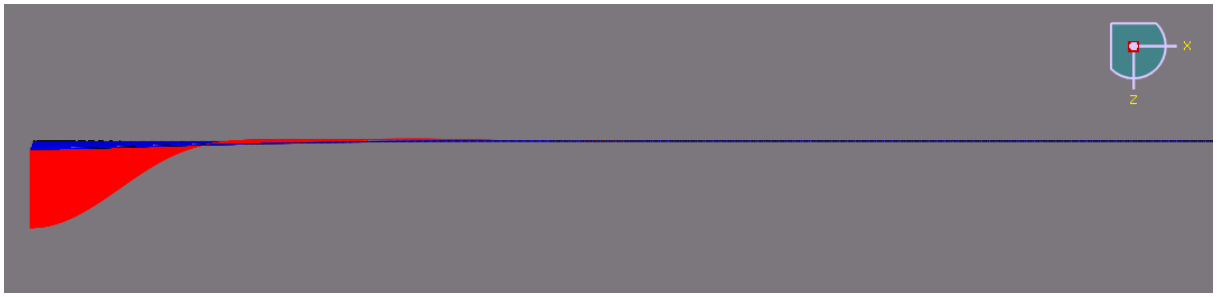

Figure 38: 10 MPa, L_o = 75 m, Δ_o = 0.9 m, U_{MAX} = 0.3 m

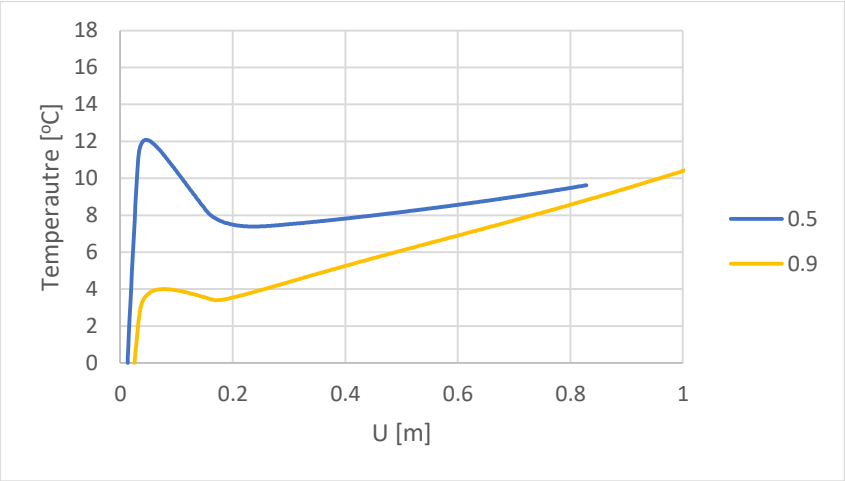

Figure 39: Temperature vs. Displacement for L_o = 50 m

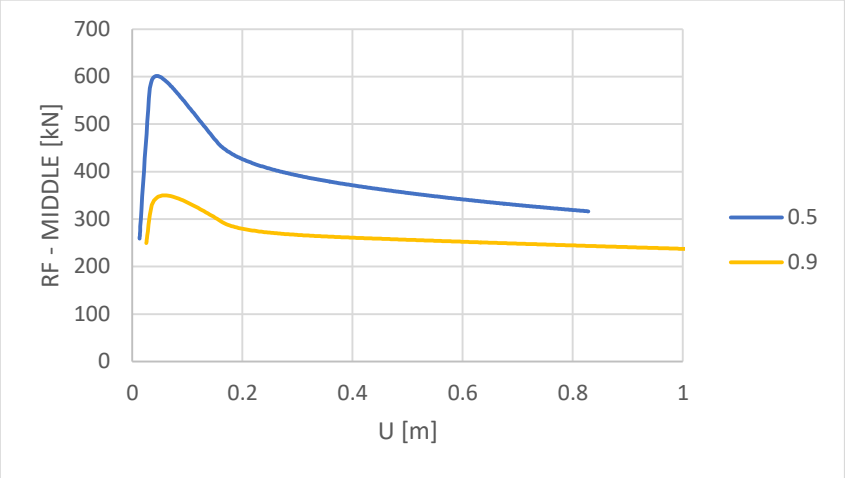

Figure 40: RF_{MIDDLE} vs. Displacement for L_o = 50 m

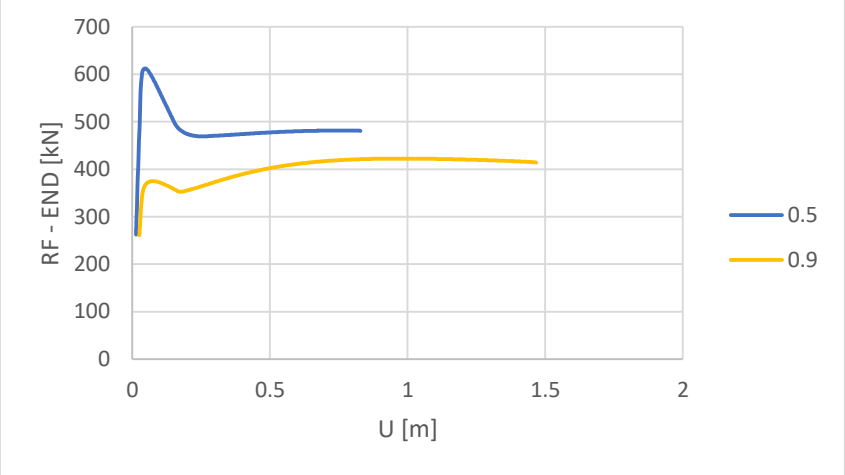

Figure 41: RF_{END} vs. Displacement for L_o = 50 m

Δ_o [m]	Maximum Temperature Load [^oC]
0.5	12.08
0.9	3.998

Table 4.2 Maximum temperature loads for initial length L_o = 50 m

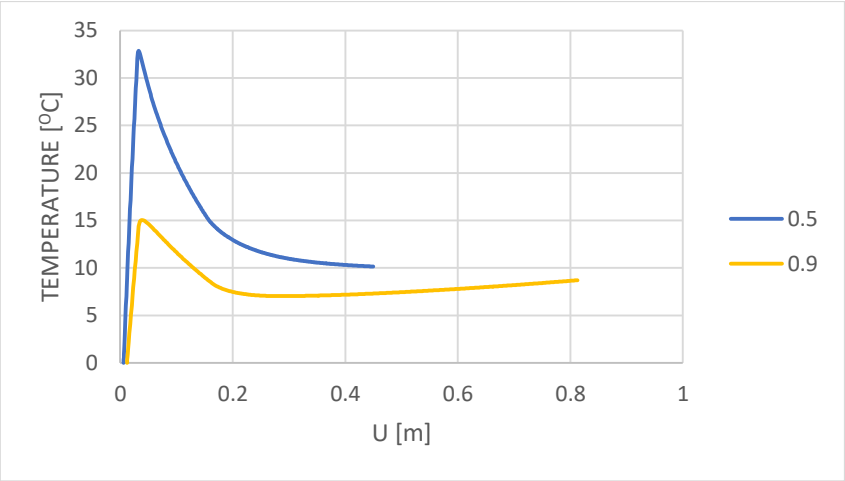

Figure 42: Temperature vs. Displacement for L_o = 75 m

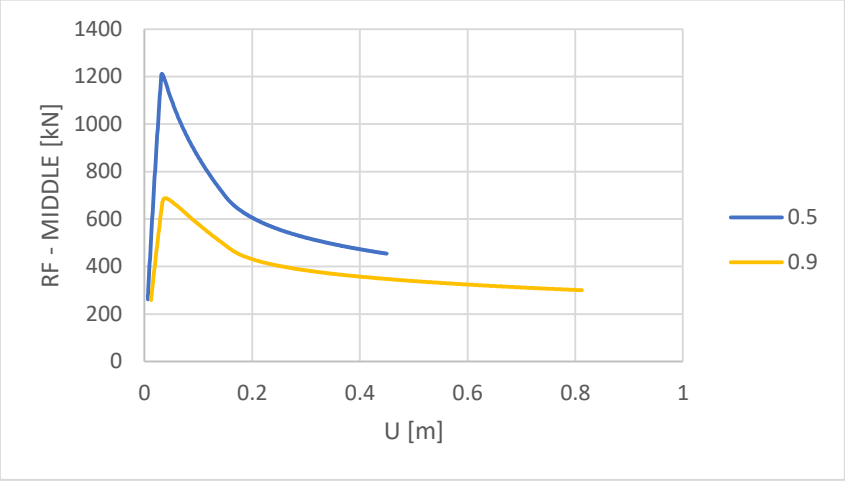

Figure 43: RF_{MIDDLE} vs. Displacement for L_o = 75 m

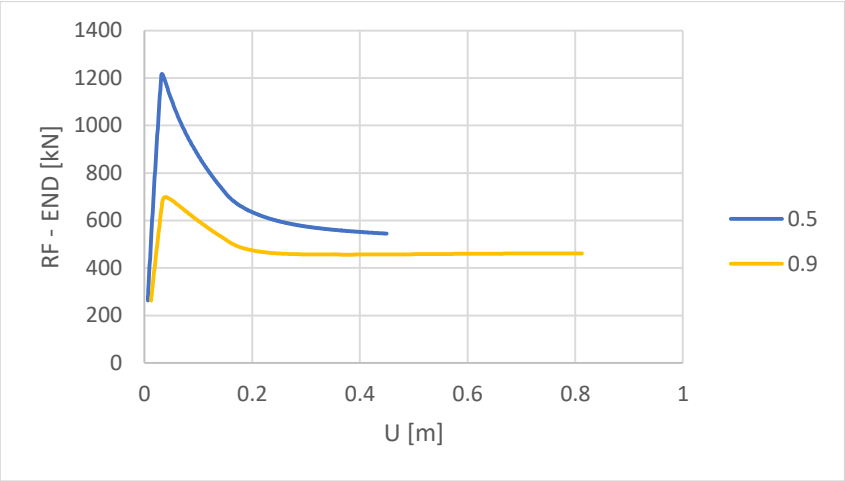

Figure 44: RF_{END} vs. Displacement for L_o = 75 m

Δ_o [m]	Maximum Temperature Load [^oC]
0.5	32.87
0.9	15.03

Table 4.3 Maximum temperature loads for initial length L_o = 75 m

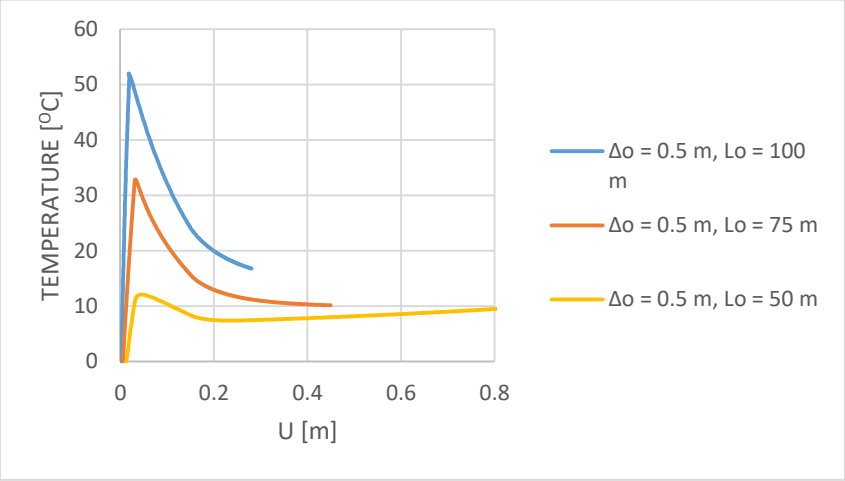

Figure 45: Temperature vs. Displacement for Δ_o = 0.5 m

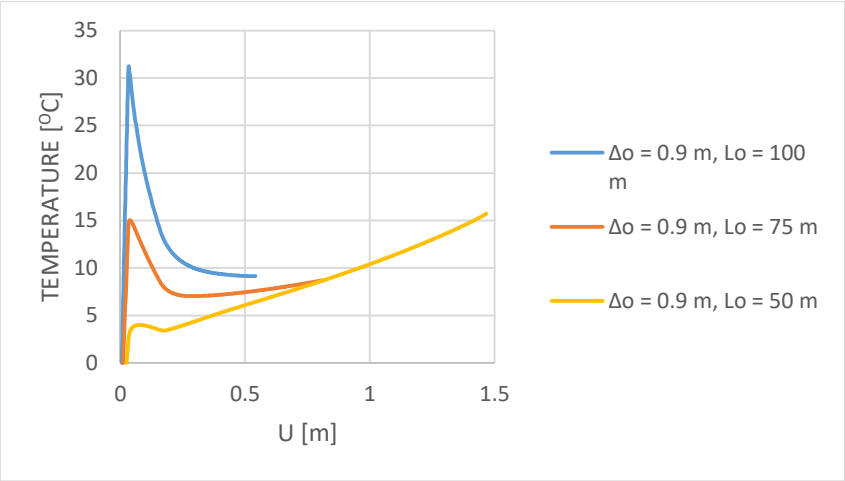

Figure 46: Temperature vs. Displacement for Δ_o = 0.9 m

In Figures 45 and 46, the temperature versus the displacement of the node with the maximum spatial displacement is plotted for all three types of initial imperfection length for Δ_o = 0.5 m and 0.9 m, respectively. A significant drop in the maximum temperature that the pipeline can withstand is observed as the initial imperfection length decreases from 100 m to 50 m. In comparison with the models in section 4.1, for 0.5 m, as L_o decreases from 100 m to 75m and from 75m to 50 m, the maximum temperature decreased from ~ 52 ^oC to ~ 32.8 ^oC and from ~ 32.8 ^oC to ~ 12 ^oC respectively. For 0.9 m, the temperature dropped from ~ 31 ^oC to ~ 15 ^oC and from ~ 15 ^oC to ~ 4 ^oC. In Figures 47 to 50, the reaction forces in the middle and the end of the pipeline are plotted for Δ_o = 0.5 m and 0.9 m and all three types of initial imperfection length. A decrease of the axial reaction forces in both ends of the pipeline is observed, which is expected from the decrease of the maximum temperature loads.

It is concluded that the initial imperfections length has a critical role in the behavior of the pipeline since a decrease of length results in a significant decrease in the pipeline's axial capacity.

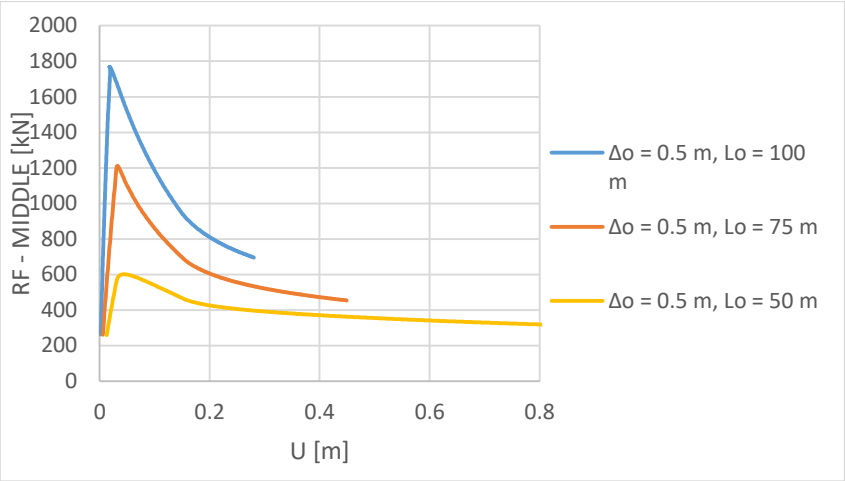

Figure 47: RF_{MIDDLE} vs. Displacement for Δ_o = 0.5 m

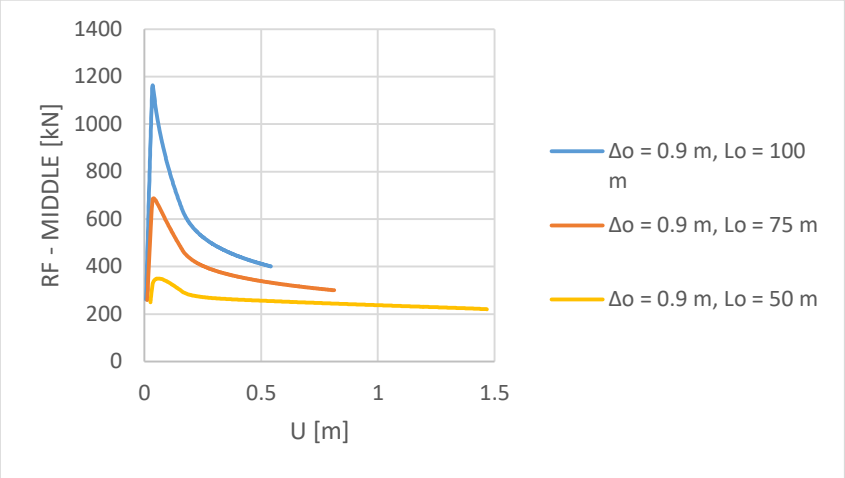

Figure 48: RF_{MIDDLE} vs. Displacement for Δ_o = 0.9 m

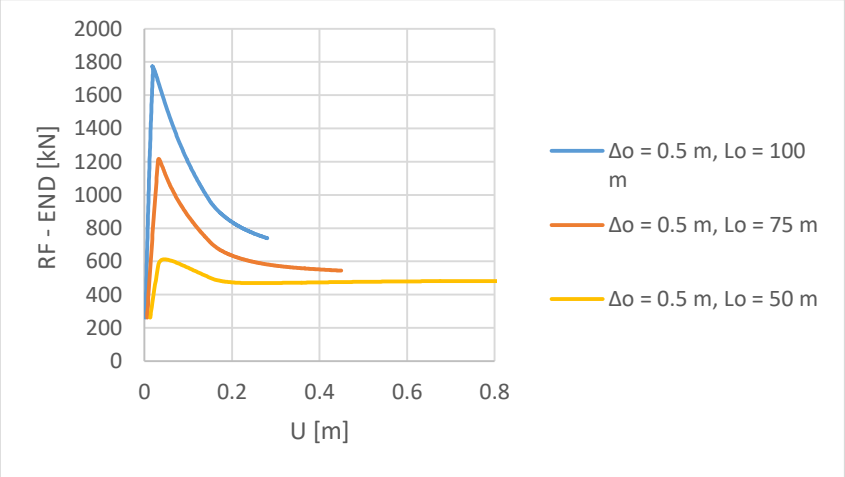

Figure 49: RF_{END} vs. Displacement for Δ_o = 0.5 m

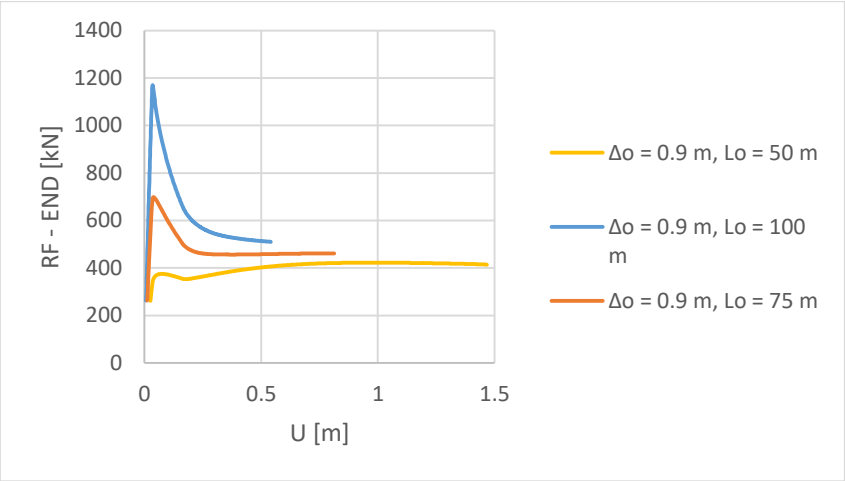

Figure 50: RF_{END} vs. Displacement for Δ_o = 0.9 m

4.3 Influence of pipeline thickness

In this section, the influence of the pipeline thickness is considered. The initial pipe's thickness of 0.5 m was changed to 0.75 and 1 in. The imperfection half-length remained constant at L_o = 100 m, and the internal pressure remained constant at 10 MPa.

Changing the pipeline thickness affects the pipe's weight, affecting the pipe–soil interaction forces in each direction. The same procedure was followed. First, a new pipeline density was calculated, taking into account the total weight and the buoyancy due to the seawater. The new density values did not vary much from the initial. Then, the weight per meter was calculated from Eq. (3.1), and the resistance force from the soil was calculated from Eq. (3.2) in each direction. The friction model, and thus the friction coefficients per direction, was not changed. In Table 4.3, the forces acting on the pipeline due to the soil resistance are displayed. In Table 4.4 and Table 4.5, the new weight of the pipeline and the geometric data for each thickness are presented, respectively. Although the density and the weight of the pipelines did not change drastically, the soil resistance increased significantly. For the definition of the pressure load, only the effective inner diameter needed to be changed.

Thickness (in.)	0.5	0.75	1
Axial (5 mm) (kN/m)	0.418	0.614	0.802
Lateral (30 mm) (kN/m)	0.836	1.228	1.603
Lateral (150 mm) (kN/m)	0.418	0.614	0.802

Table 4.4 Resistance force acting on the pipeline per unit length

Thickness (in.)	0.5	0.75	1
Total Weight (kN / m)	0.836	1.228	1.603
Total Weight (kN / m^3)	67.345	67.326	67.316

Table 4.5 Weight of pipeline per unit length and cubic meter

Pipe Thickness t (in.)	0.5	0.75	1
Pipe outer diameter Do (in)	12.75	12.75	12.75
Pipe inner diameter Pipe inner diameter Di (in)	11.75	11.25	10.75
Do / t	25.5	17	12.75

Table 4.6: Geometric data for 0.5, 0.75, and 1 in. thickness

Figures 51 to 56 show a top-down view of the shape of the pipeline at the point of the analysis where the maximum lateral displacement is equal to 0.3 m for both types of thicknesses. The red color shows the displacement of each node, and the blue color is the initial shape of the pipeline before the analysis begins. For 0.75 in., the buckle begins to grow at the center of the pipeline, at the same place where the initial imperfection was placed. The same behavior is observed in the 1 in. models as well. The only difference is found in the model with an initial width of 0.7 m. The pipe buckles near the imperfection, but the maximum displacement is approximately 18 m to the left and not at the middle node.

In Figures 57, 58, and 59, the temperature load and the reaction forces at the end of the pipe versus the displacement of the node with the maximum spatial displacement are plotted for a pipe thickness of 0.75 in. Similarly, in Figures 60, 61, and 62, the temperature load and the reaction forces are plotted for a pipe thickness of 1 in. For 0.75 in. the temperature load behaves the same way with the increase of the imperfections width, the maximum temperature that the pipe can withstand before buckling decreases. The reaction forces increase, reach the maximum axial capacity of the pipeline, and drop to a constant value. The pipeline of a thickness of 1 in. has the same behavior as for 0.75 in. The only difference is found in the buckling mode for a width of 0.7m. Since the maximum displacement is not spotted at the same node as the rest models, the Temperature vs. Displacement curve stands out but has the same form as the rest. In Tables 4.6 and 4.7, the maximum temperatures are shown. Table 4.8 shows the maximum loads for the results of section 4.1.

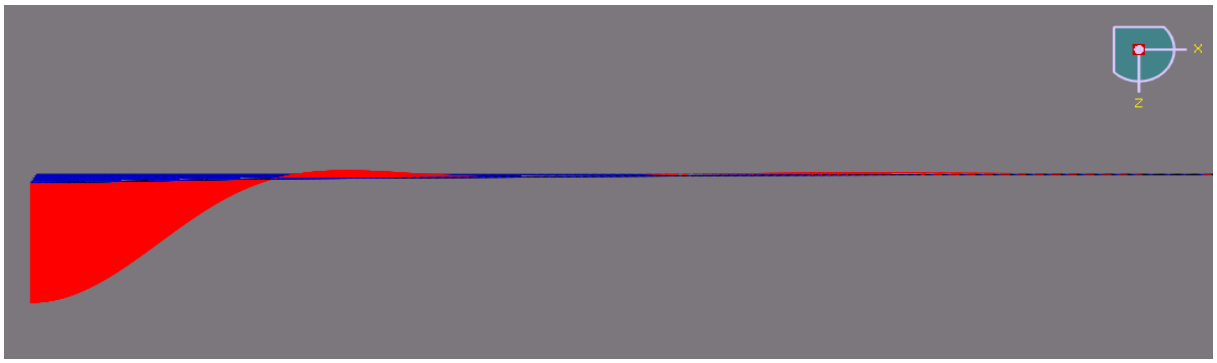

Figure 51: 10 MPa, L_o = 100 m, Δ_o = 0.5 m, t = 0.75 in., U_{MAX} = 0.3 m

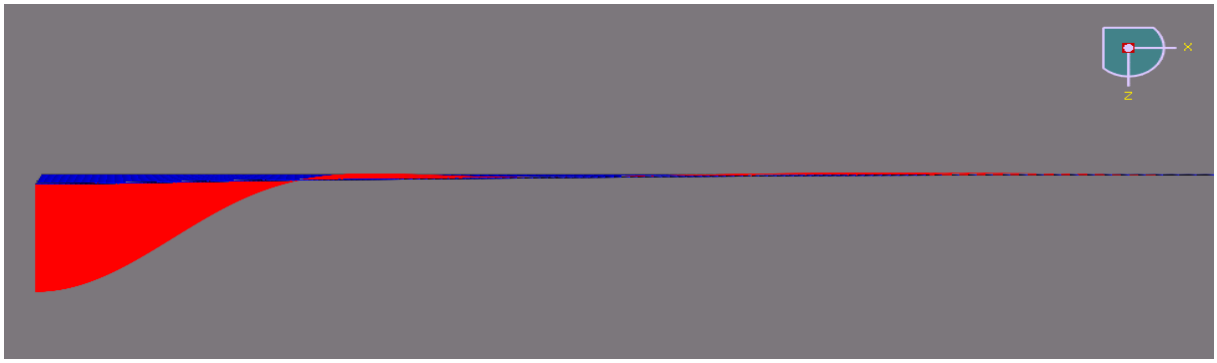

Figure 52: 10 MPa, L_o = 100 m, Δ_o = 0.7 m, t = 0.75 in., U_{MAX} = 0.3 m

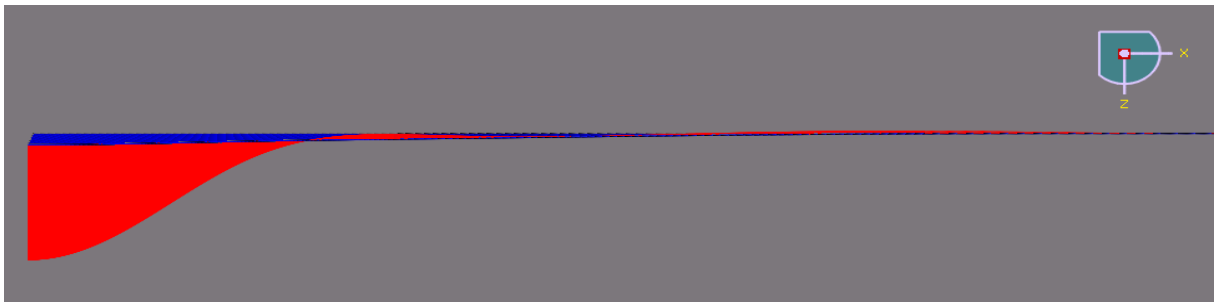

Figure 53: 10 MPa, L_o = 100 m, Δ_o = 0.9 m, t = 0.75 in., U_{MAX} = 0.3 m

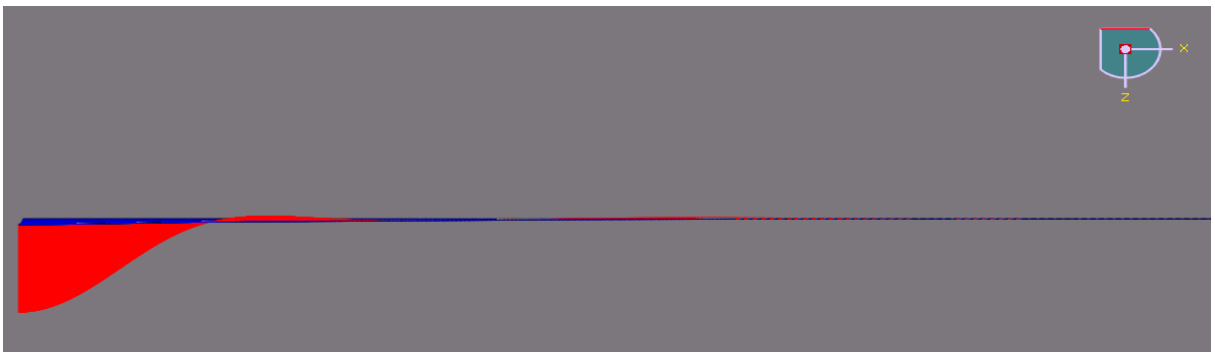

Figure 54: 10 MPa, L_o = 100 m, Δ_o = 0.5 m, t = 1 in., U_{MAX} = 0.3 m

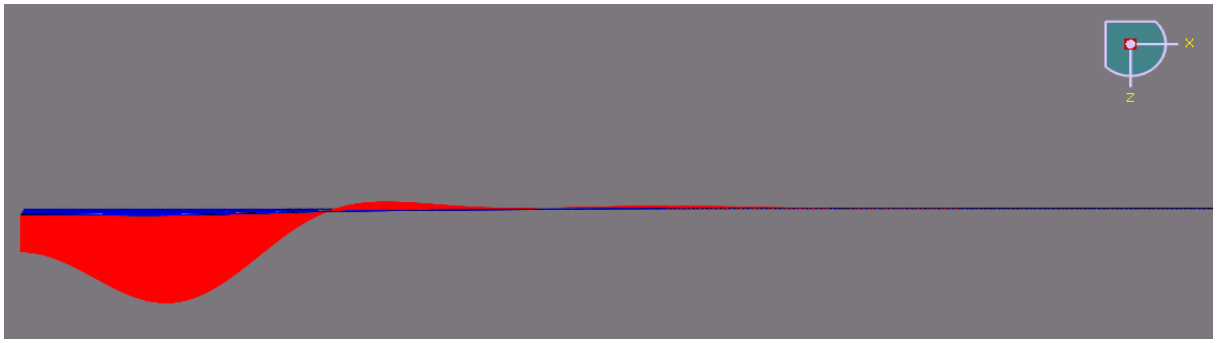

Figure 55: 10 MPa, L_o = 100 m, Δ_o = 0.7 m, t = 1 in., U_{MAX} = 0.3 m

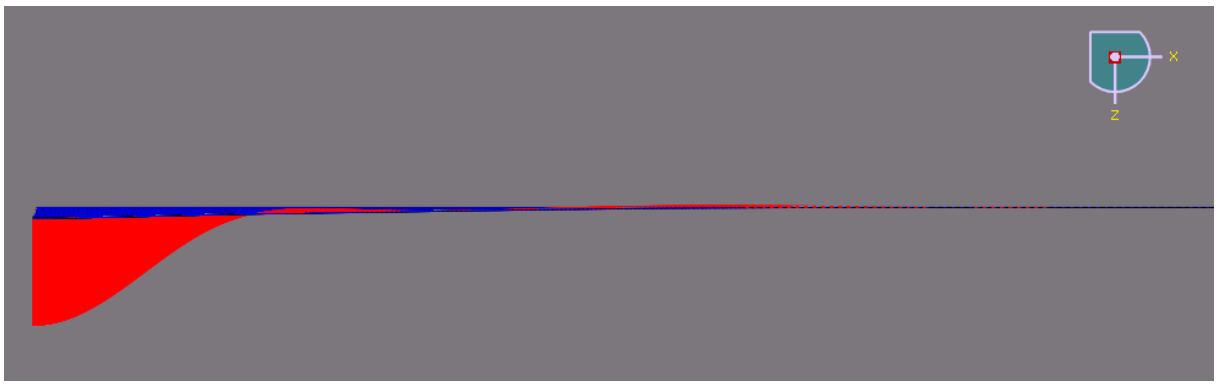

Figure 56: 10 MPa, L_o = 100 m, Δ_o = 0.9 m, t = 1 in., U_{MAX} = 0.3 m

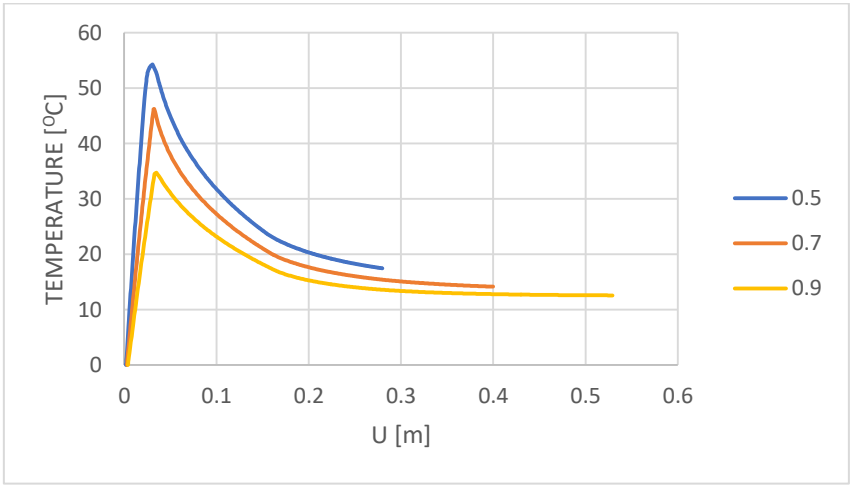

Figure 57: Temperature vs. Displacement for t = 0.75 in.

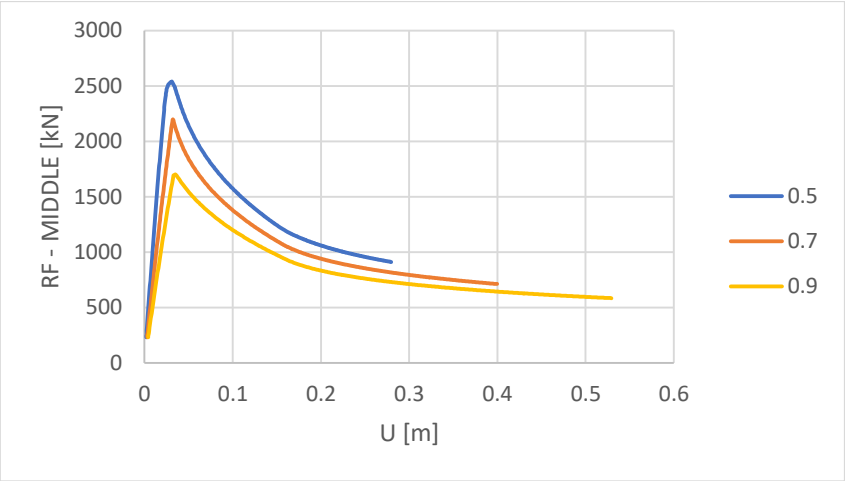

Figure 58: RF_{MIDDLE} vs. Displacement for t = 0.75 in.

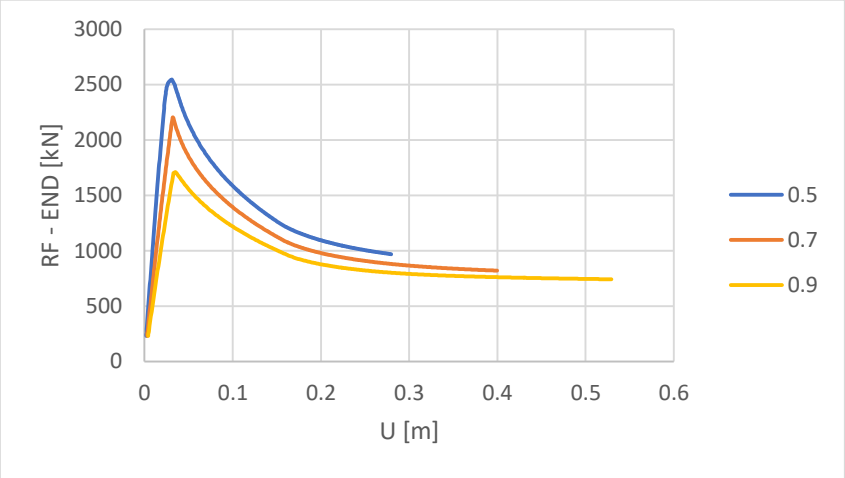

Figure 59: RF_{END} vs. Displacement for t = 0.75 in.

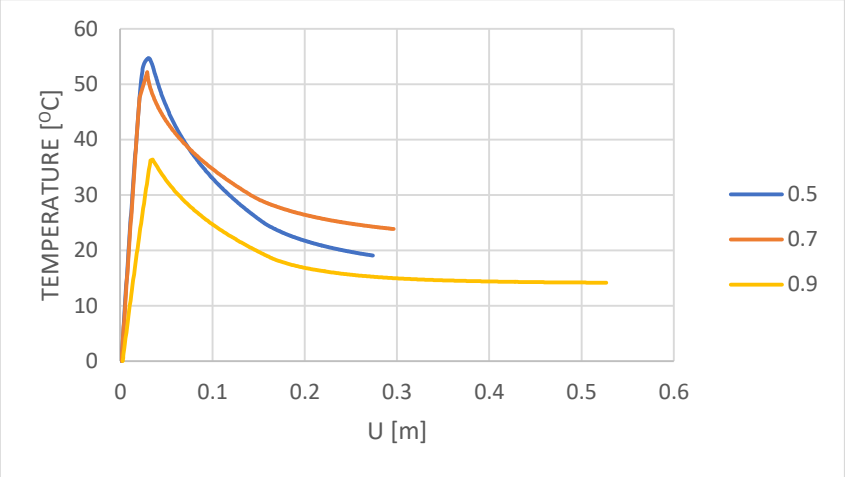

Figure 60: Temperature vs. Displacement for t = 1 in.

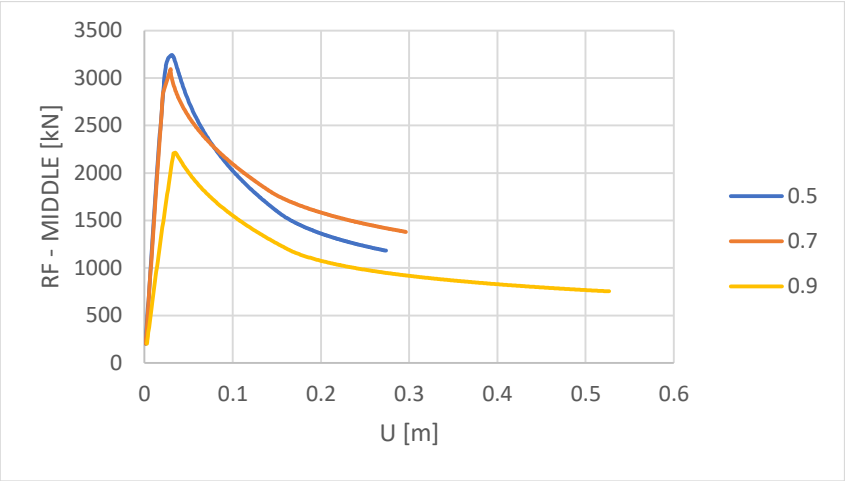

Figure 61: RF_{MIDDLE} vs. Displacement for t = 1 in.

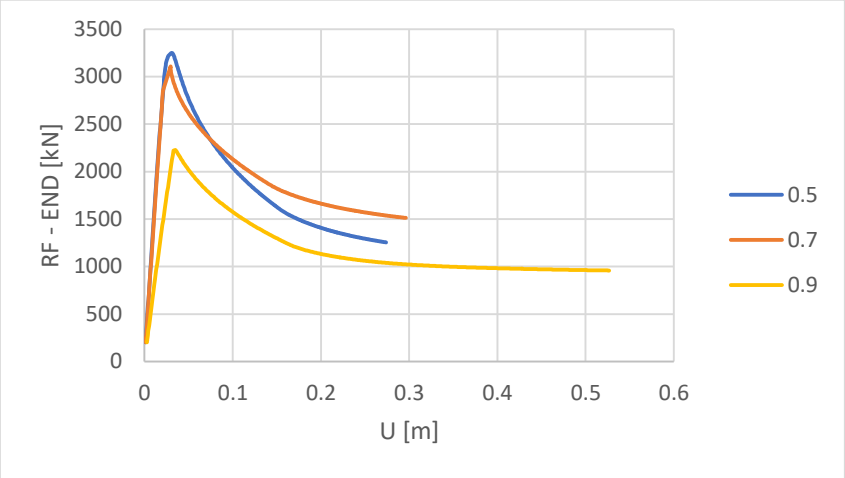

Figure 62: RF_{END} vs. Displacement for t = 1 in.

Δ_o [m]	Maximum Temperature Load [^oC]
0.5	54.238
0.7	46.252
0.9	34.702

Table 4.7 Maximum temperature loads for t = 0.75 in.

Δ_o [m]	Maximum Temperature Load [^oC]
0.5	54.713
0.7	52.159
0.9	36.392

Table 4.8 Maximum temperature loads for t = 1 in.

Δ_o [m]	Maximum Temperature Load [^oC]
0.5	51.987
0.7	42.646
0.9	31.235

Table 4.9 Maximum temperature loads for t = 0.5 in.

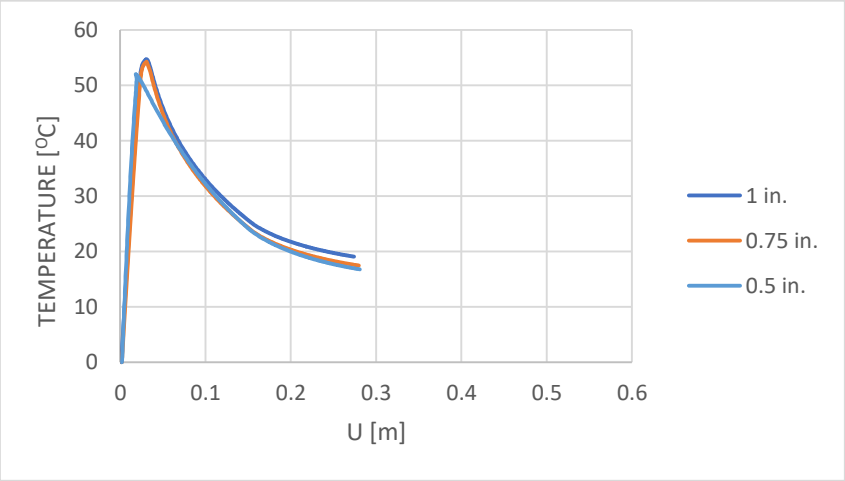

Figure 63: Temperature vs. Displacement for Δ_o = 0.5 m

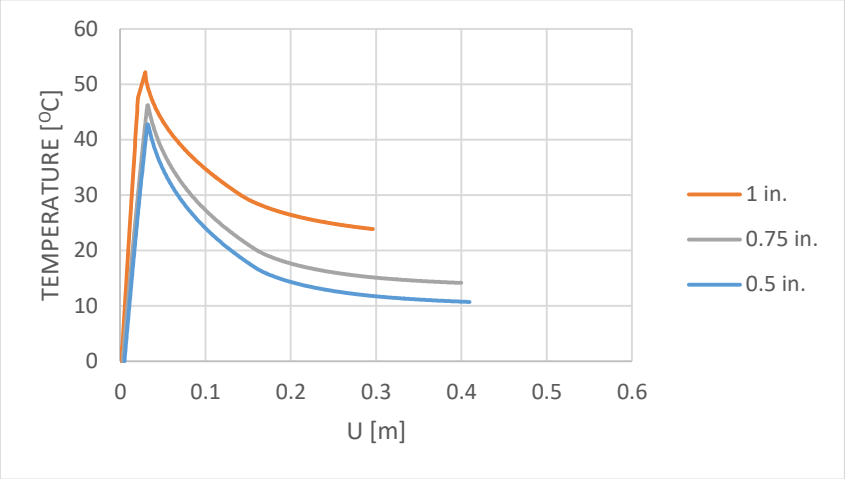

Figure 64: Temperature vs. Displacement for Δ_o = 0.7 m

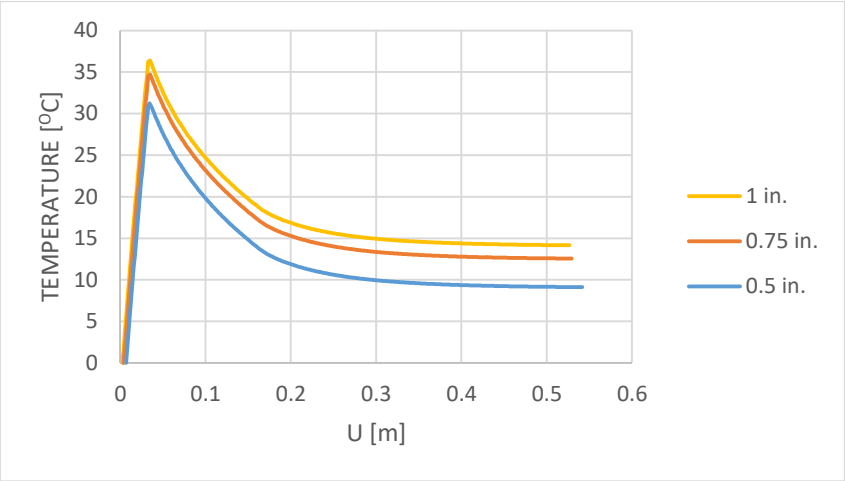

Figure 65: Temperature vs. Displacement for Δ_o = 0.9 m

In Figures 63, 64, and 65, the temperature versus the displacement of the node with the maximum spatial displacement is plotted for all three types of pipe thickness for Δ_o = 0.5 m, 0.7 m, and 0.9 m, respectively. Compared with the results of section 4.1, for Δ_o = 0.5 m, the maximum temperature does not decrease significantly and remains almost constant when moving from a 1 in. to a 0.75 in. pipeline. For Δ_o = 0.7 and 0.9 m, the maximum temperature decreases as the pipe thickness decreases but not drastically. For 0.7 m, there is a drop of 13 % in temperature when decreasing the pipe thickness from 1 to 0.75 in. For 0.5 in. the decrease in temperature when moving from a 1 in. pipe to a 0.75 in. pipe is slight, about 1%. The rest present a reduction by approximately 5-10 % when the thickness varies from 0.5 to 0.75 in. and from 0.75 to 1 in. The maximum temperatures per thickness and imperfection width are displayed in Figure 66.

Although the maximum temperatures do not vary remarkably with the pipe thickness, the reaction forces in the middle and the end node of the pipeline drop significantly as the thickness decreases. In Figures 67 to 72, the reaction forces at the middle and end of the pipeline for all three types of pipe thickness and initial imperfection widths are plotted.

It is concluded that the increase of the thickness of the pipe increases the maximum temperature that the pipeline can withstand before beginning to buckle, but the change is not significant. More notable is the decrease in the reaction forces acting on the pipeline's middle and end node.

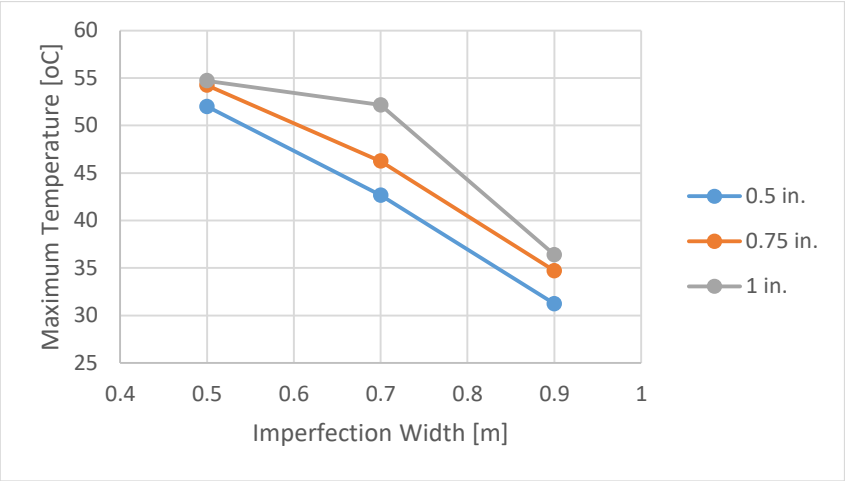

Figure 66: Maximum Temperatures for 0.5, 0.75, and 1 in. thick pipe

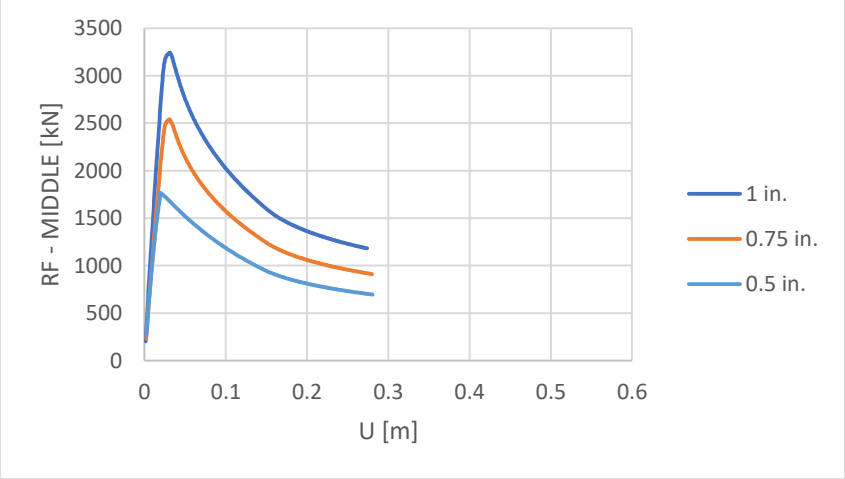

Figure 67: RF_{MIDDLE} vs. Displacement for Δ_o = 0.5 m

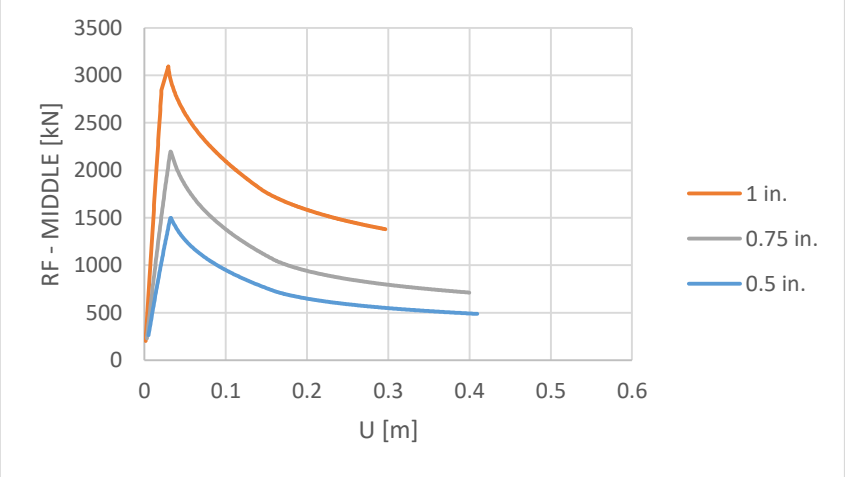

Figure 68: RF_{MIDDLE} vs. Displacement for Δ_o = 0.7 m

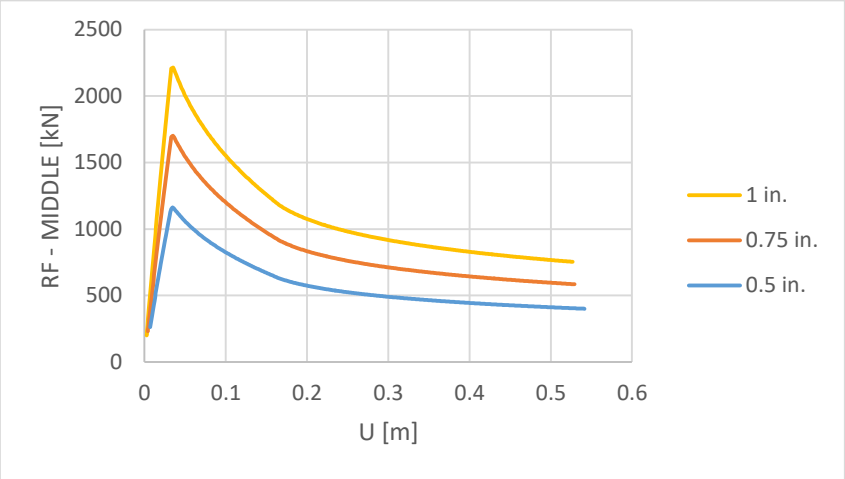

Figure 69: RF_{MIDDLE} vs. Displacement for Δ_o = 0.9 m

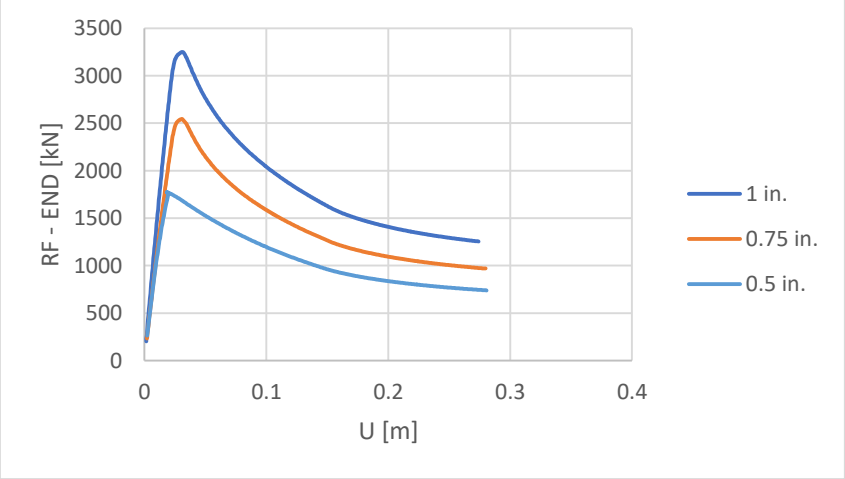

Figure 70: RF_{END} vs. Displacement for Δ_o = 0.5 m

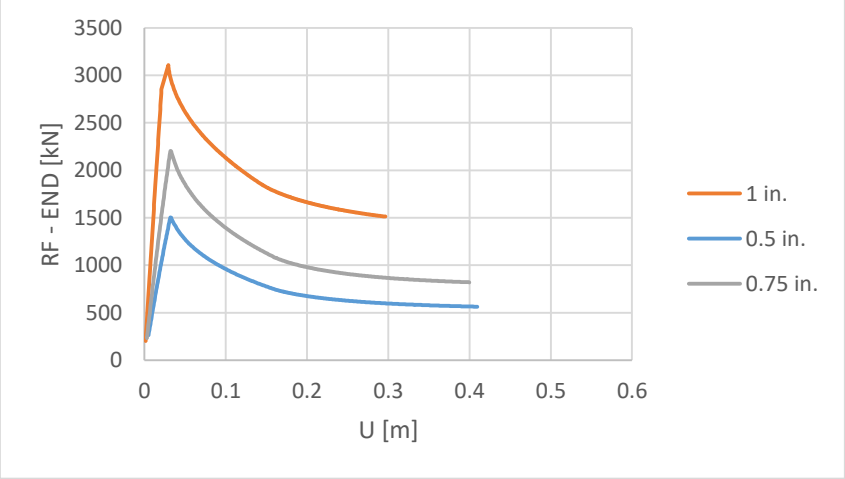

Figure 71: RF_{END} vs. Displacement for Δ_o = 0.7 m

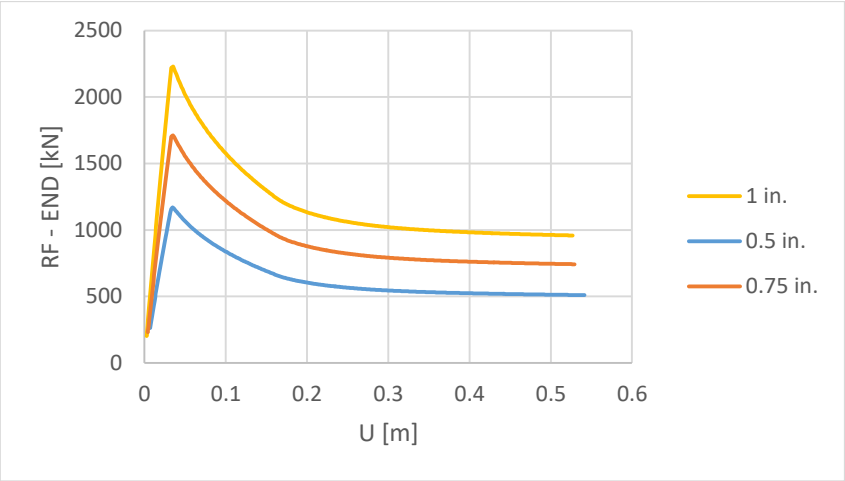

Figure 72: RF_{END} vs. Displacement for Δ_o = 0.9 m

4.4 Influence of internal pressure

Finally, the effect of the internal pressure on the behavior of the pipeline was tested. For a constant half-length of L_o = 100 m and a width of Δ_o = 0.5, 0.7, 0.9, the applied pressure was decreased to 5 MPa.

All the previous analyses were done with an internal pressure of 10 MPa, which is about 23 % of the yield stress. With the reduction of the internal pressure, an increase in the load needed for the pipe to buckle is expected since the axial load due to internal pressure will be reduced.

Figures 73 to 75 show a top-down view of the shape of the pipeline at the point of the analysis where the maximum lateral displacement is equal to 0.2 m. The red color shows the displacement of each node, and the blue color is the initial shape of the pipeline before the analysis begins. For all widths of initial imperfection, the buckle grows in the middle of the pipeline, where the initial imperfection is placed, and the middle node is the node with the maximum spatial displacement.

In Figures 76 through 78, the load and the reaction forces versus the displacement of the node with the maximum displacement are plotted. The maximum temperature load that the pipe can withstand before buckling begins decreases as the initial imperfection width increases. The reaction forces act the same way decreasing with the increase of width. In Table 4.9, the maximum temperatures per model are displayed.

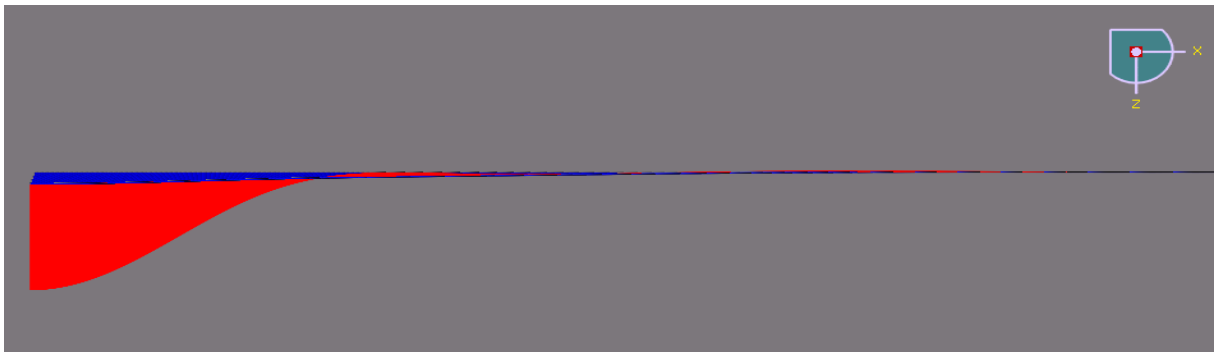

Figure 73: 5 MPa, L_o = 100 m, Δ_o = 0.5 m, U_{MAX} = 0.2 m

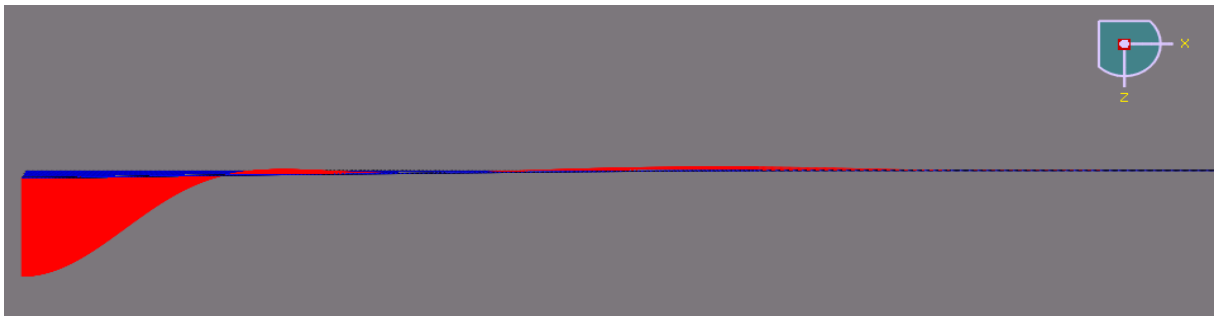

Figure 74: 5 MPa, L_o = 100 m, Δ_o = 0.7 m, U_{MAX} = 0.2 m

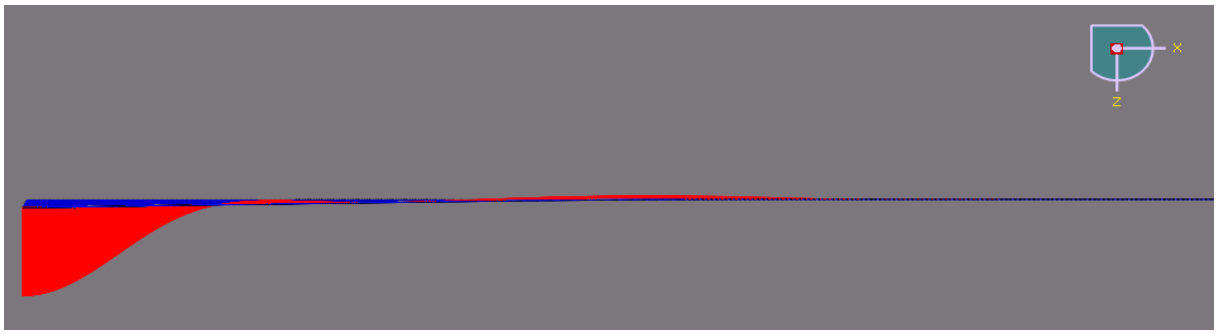

Figure 75: 5 MPa, L_o = 100 m, Δ_o = 0.9 m, U_{MAX} = 0.2 m

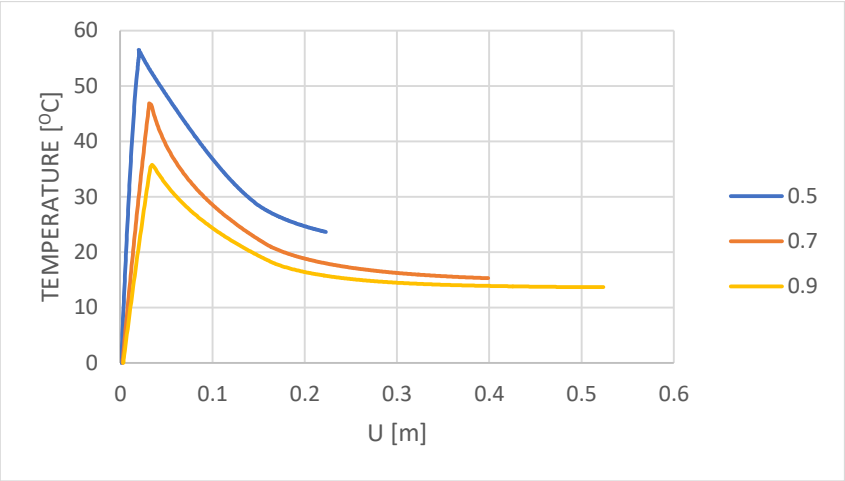

Figure 76: Temperature vs. Displacement for p = 5 MPa

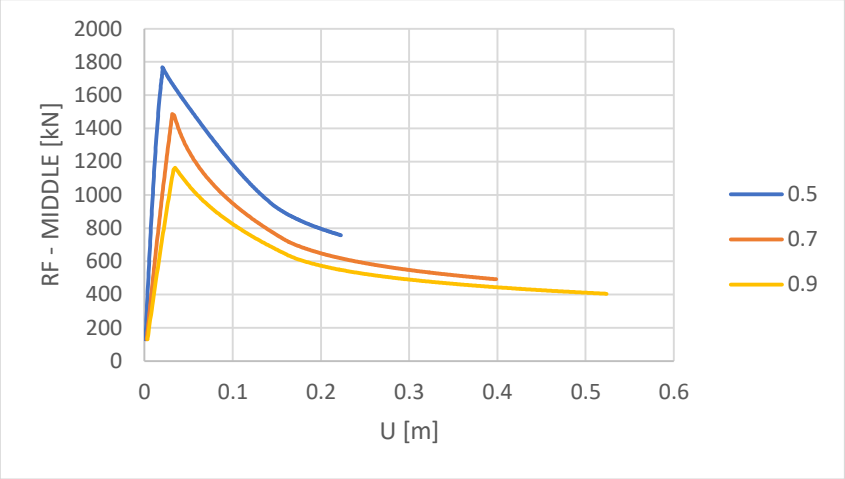

Figure 77: RF_{MIDDLE} vs. Displacement for p = 5 MPa

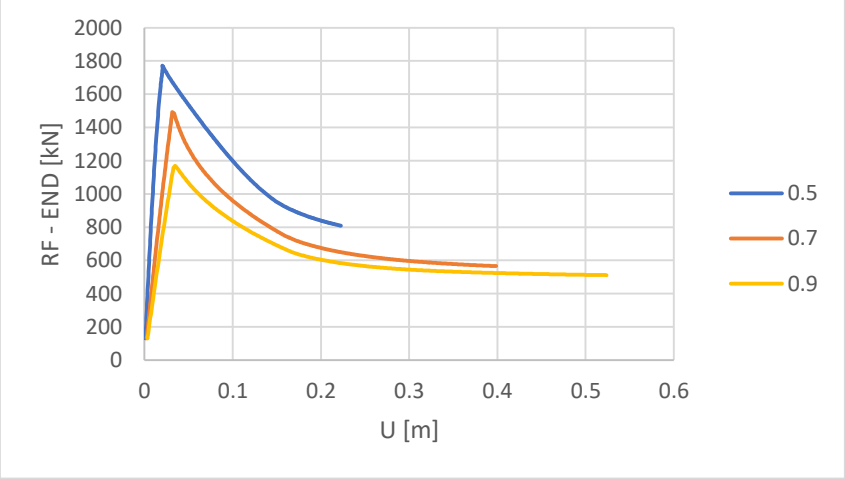

Figure 78: RF_{END} vs. Displacement for p = 5 MPa

Δ_o [m]	Maximum Temperature Load [^oC]
0.5	56.511
0.7	46.888
0.9	35.772

Table 4.10 Maximum temperature loads for p = 5 MPa

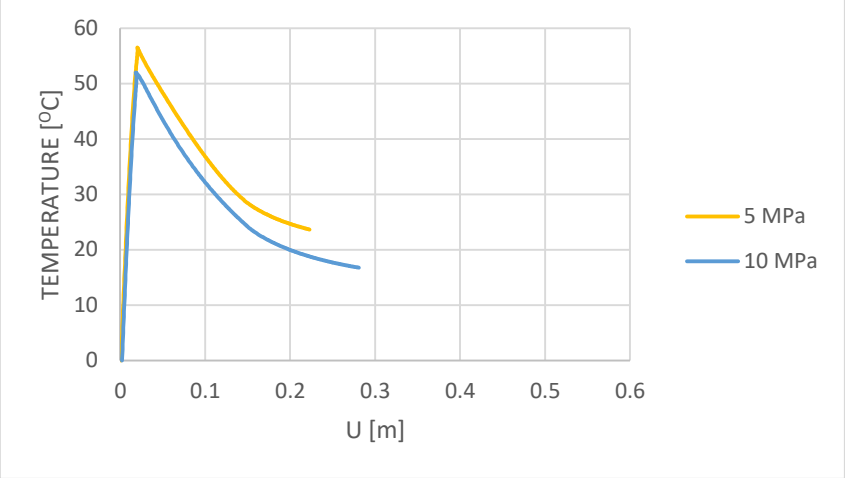

Figure 79: Temperature vs. Displacement for Δ_o = 0.5 m

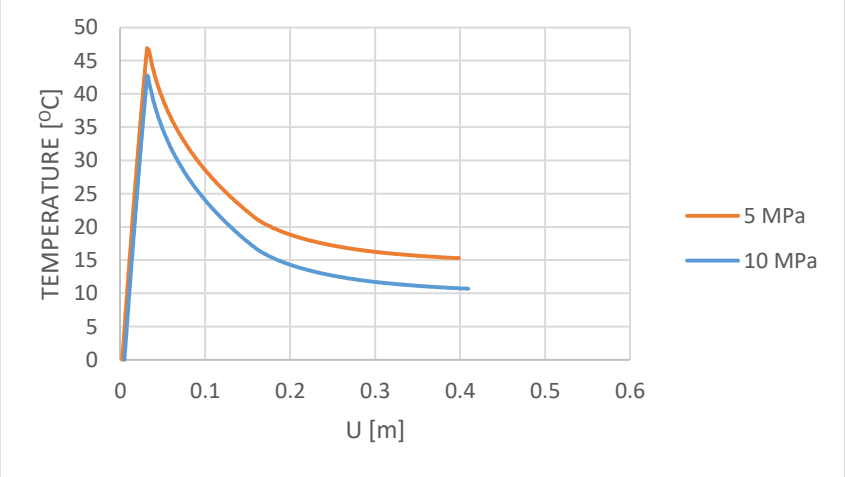

Figure 80: Temperature vs. Displacement for Δ_o = 0.7 m

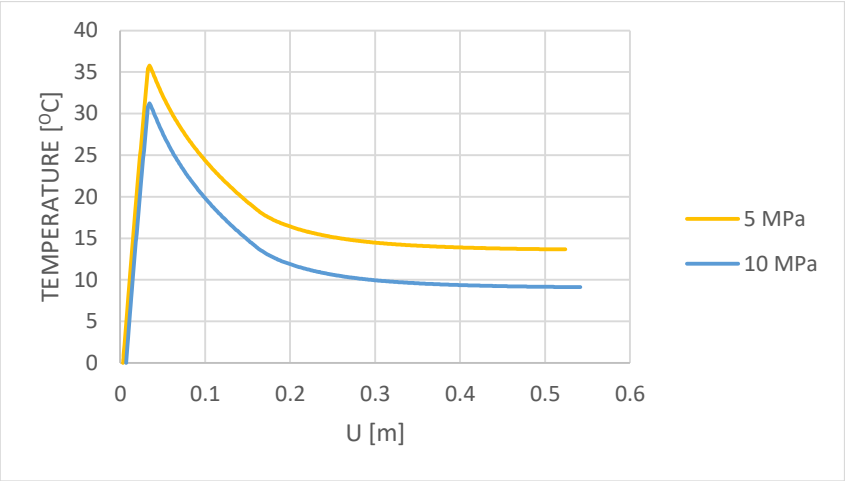

Figure 81: Temperature vs. Displacement for Δ_o = 0.9 m

In Figures 79, 80, and 81, the temperature versus the displacement of the node with the maximum spatial displacement is plotted for an internal pressure of 5 and 10 MPa for Δ_o = 0.5 m, 0.7 m, and 0.9 m, respectively. As expected, with the reduction of the internal pressure of the pipe, the maximum temperature increases. Compared with the results from section 4.1, for the initial imperfection of 0.5 m, the temperature increases by 8.65 % from ~ 52 ^{o}C to ~ 56.5 ^{o}C. For Δ_o = 0.7 m, it increases by 10 % from ~ 42.7 ^{o}C to ~ 47 ^{o}C and for Δ_o = 0.9 m, the temperature increases by 12.9 % from ~ 31 ^{o}C to ~ 35.7 ^{o}C.

In Figures 82 through 87, the reaction forces at the middle and the end node of the pipeline are plotted. No reduction or increase is observed for any case of initial imperfection or internal pressure.

It is concluded that an increase in the internal pressure of the pipeline can decrease the lateral buckling resistance, but it does not affect the reaction forces at the pipeline end and middle node.

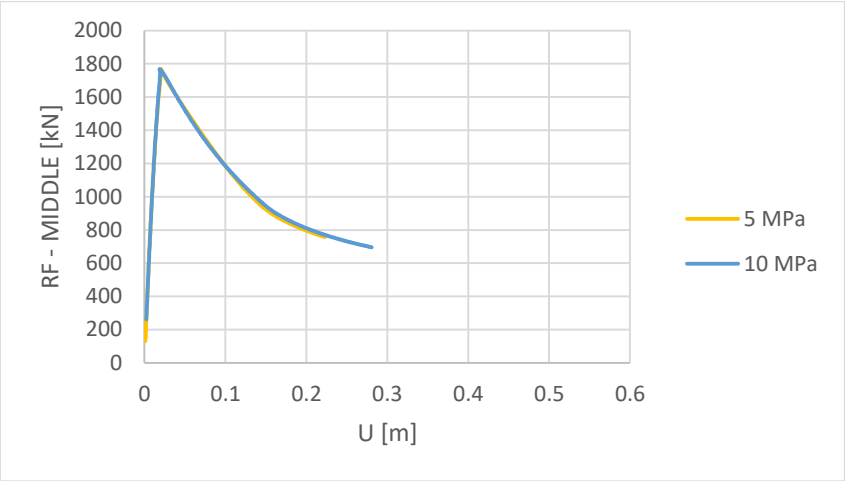

Figure 82: RF_{MIDDLE} vs. Displacement for Δ_o = 0.5 m

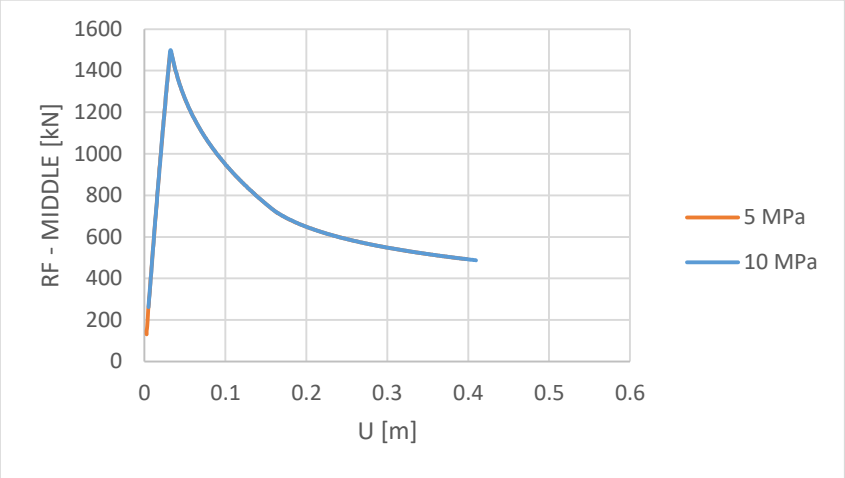

Figure 83: RF_{MIDDLE} vs. Displacement for Δ_o = 0.7 m

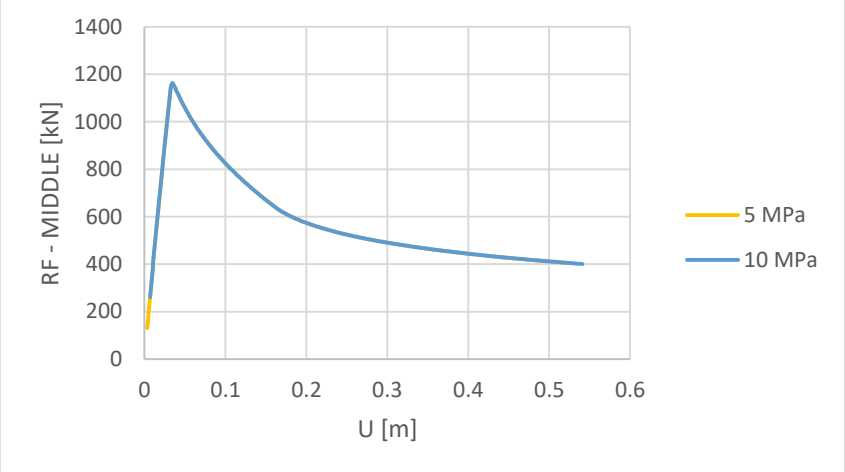

Figure 84: RF_{MIDDLE} vs. Displacement for Δ_o = 0.9 m

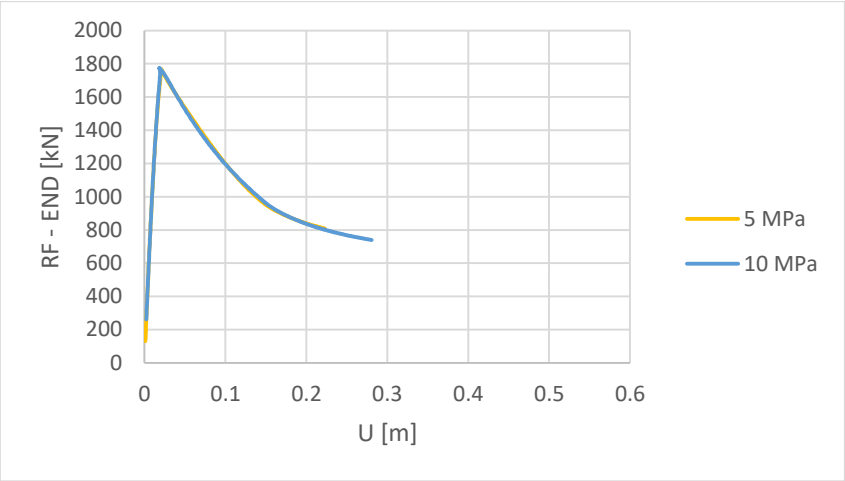

Figure 85: RF_{END} vs. Displacement for Δ_o = 0.5 m

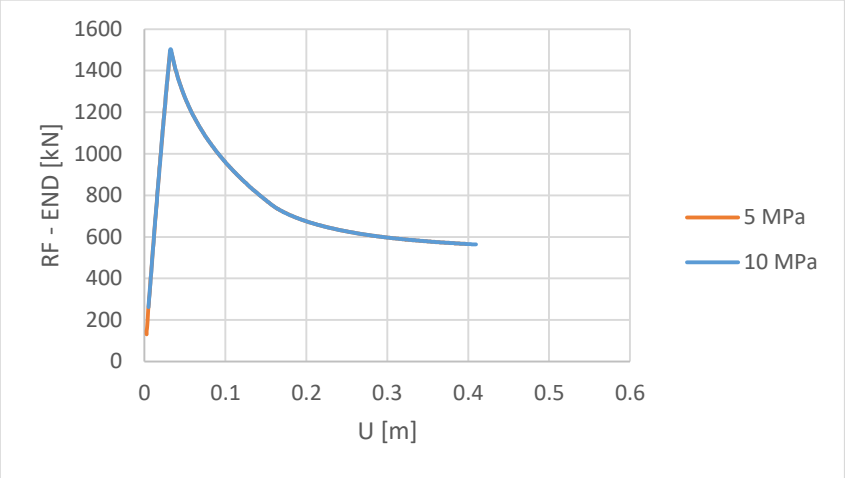

Figure 86: RF_{END} vs. Displacement for Δ_o = 0.7 m

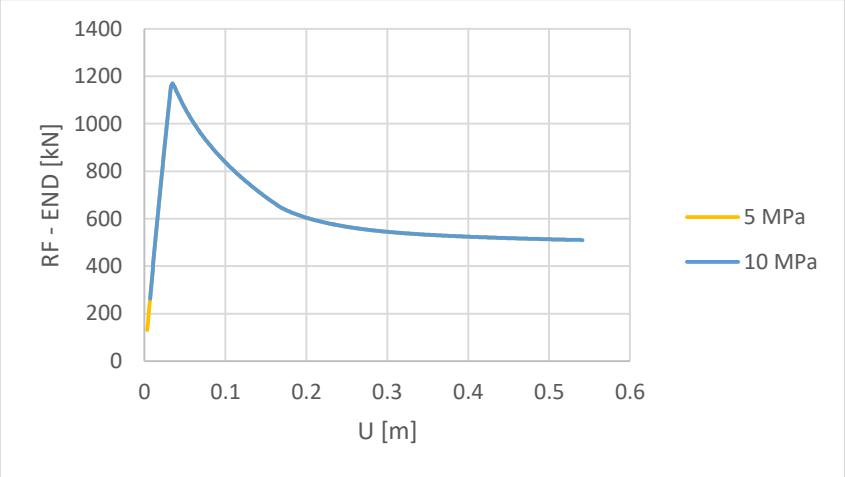

Figure 87: RF_{END} vs. Displacement for Δ_o = 0.9 m

Chapter 5. CONCLUSIONS – SUGGESTIONS FOR FURTHER STUDY

5.1 Conclusions

Offshore pipelines are used widely for the transportation of hydrocarbons or hot oils in great depths. Strong axial compressive forces due to pressure and temperature changes are created that can lead to the pipeline's global or local buckling. This thesis focused on steel pipelines placed on the sea bed that are subjected to lateral buckling.

Lateral buckling can be used to control the behavior of the pipeline as long as it occurs in a controlled manner. In this Thesis, Finite element models are developed to assess these systems' behavior under high pressure and high-temperature conditions for various initial imperfections widths, internal pressures, and temperature values.

Firstly, concerning the finite element analyses on the effect of the initial imperfection's width, the results show that:

- The maximum temperature load that the pipe can withstand decreases as the initial imperfections width increases.
- The resulting reaction forces both in the center and at the end of the pipeline decrease when the initial imperfection's width is increased.
- The maximum displacement is at the center of the pipeline, where the initial imperfection's width is the maximum, except for the model with an imperfection width of 0.5 m where the maximum displacement is found approximately 74 m to the left of the pipe's center of symmetry.

Then the effect of the imperfection length was studied. The results show that:

- The decrease of the imperfections length causes a significant reduction to the maximum temperature that causes the pipeline to begin to buckle.
- The resulting reaction forces decrease with the decrease of the imperfection's initial length.
- The maximum displacement is at the pipeline center, where the initial imperfection's width is the maximum.

Regarding the effect of the thickness of the pipe on the results:

- The maximum temperature that the pipeline can withstand increases slightly with the increase of the pipeline thickness.
- The reaction forces decrease with the increase of the pipeline thickness.
- All the models begin buckling at the center of the pipeline. The node with the maximum displacement is the center node except for the model with, $\Delta o = 0.7$ m and t = 1 in where the maximum displacement is located a few meters to the right.

Finally, with the decrease of the operating pressure of the pipe:

- The increase of internal pressure can decrease the lateral buckling resistance.
- The decrease of the pipeline's operating pressure does not affect the reaction forces at the middle and end node of the pipeline.
- For all the cases of imperfection width and internal pressure, the buckle forms in the same region, near the center of the pipeline, and the middle node has the maximum spatial displacement.

5.2 Recommendations for further work

Some of the questions that have remained unanswered and could be the subject of further work are the effects of:

- Different types of initial imperfections
- Pipe coating
- Residual Stresses
- Soil Stiffness – Different Model
- Effect of temperature on the material properties

on the post-buckling behavior of the pipeline and the stresses created during the analyses.

REFERENCES

[1] Bruton, D. A. S., (2008) Safe Design of Hot On-Bottom Pipelines with Lateral Buckling. Presentation at the *Clarom Seminar*, Paris, June 5, 2008

[2] Randolph, M. F., White, D. J., and Yan, Y., (2012), Modelling the axial resistance on deep-water pipelines, *Géotechnique,* 62 (9), 837-846.

[3] White, D. J. and Dingle, H. R. C., (2011), The mechanism of steady friction between seabed pipelines and clay soils, *Géotechnique,* 61 (12), 1035-1041.

[4] Miles, D. J. and Calladine, C. R., (1999), Lateral Thermal Buckling of Pipelines on the Sea Bed, *Journal of Applied Mechanics*, 66 (4), 891-897.

[5] Den, H.J.P. Beams on Elastic Foundation. In *Advanced Strength of Materials*, *Dover Publications*, Inc., Mineola, New York, 141-170, 1987.

[6] Kyriakides, S. and Zhang, W., (2021), Controlled pipeline lateral buckling by reeling induced curvature imperfections, *Marine Structures*, 77, 102905

[7] White, D.J., Ganesan S.A., Bolton, M.D., Bruton, D.A.S, Ballard J-C. and Langford T. SAFEBUCK JIP - Observations of Axial Pipe-soil Interaction from Testing on Soft Natural Clays. Paper presented at the *Offshore Technology Conference*, Houston, Texas, USA, May 2-5, 2011.

[8] Ju, G. T. and Kyriakides, S., (1988), Thermal Buckling of Offshore Pipelines, *Journal of Offshore Mechanics and Arctic Engineering,* 110 (4), 355-364.

[9] Florian GOUNEAU, (2007), *Global Buckling of Submarine Pipelines*, MSc Thesis, School of Applied Sciences, Cranfield University.

[10] Hobbs, R.E. (1984) In-Service Buckling of Heated Pipelines, *J. Transp. Eng.*,110 (2), 175-189

[11] Karampour, H., Albermani, F. and Gross, J., (2013), On lateral and upheaval buckling of subsea pipelines, *Engineering Structures*, 52, 317-330

[12] Seyfipour, I., Walker, A. and Kimiaei, M., (2019), Local buckling of subsea pipelines as a walking mitigation technique, *Ocean Engineering,* 194, 106626

[13] Gallegillo, M., Qi, X., Ofoha, G., Bhide, R., Messias, N. and Helland, T. Post-Reeled Behaviour of Pipelines With Global Buckling Mitigation by the Residual Curvature Method. In *Proceedings of the ASME 2017 36th International Conference on Ocean, Offshore and Arctic Engineering. Trondheim*, Norway. June 25–30, 2017.

[14] Collberg, L., Carr, M., Levold, E. (2011) Safebuck Design Guideline and DNV-RP-F110. Paper presented at the *Offshore Technology Conference*, Houston, TX, May 2-5, 2011

[15] Abaqus/Standard, Solution Technology for Static and Low-speed Dynamic Events. *Dassault Systèmes®,* [www.3ds.com/products-services/simulia/products/abaqus/abaqusstandard/, accessed 05/07/2021].

[16] Smith, M. (2014), Abaqus/CAE User's Guide, Version 6.14. Dassault Systèmes Simulia Corp, Providence, RI. [http://130.149.89.49:2080/v6.14/books/usi/default.htm]

[17] Smith, M. (2016), Abaqus Keywords Reference Guide. Dassault Systèmes Simulia Corp, Providence, RI. [http://130.149.89.49:2080/v2016/books/key/default.htm?startat=ch06abk01.html]